Paleogene tropical Pacific: Clues to circulation, productivity, and plate motion

T. C. Moore Jr.,[1] Jan Backman,[2] Isabella Raffi,[3] Catherine Nigrini,[1] Annika Sanfilippo,[4] Heiko Pälike,[3] and Mitchell Lyle[5]

Received 5 December 2003; revised 19 May 2004; accepted 10 June 2004; published 18 September 2004.

[1] Stratigraphic data from 63 Deep Sea Drilling Project and Ocean Drilling Program (ODP) sites that sample the lower Neogene and Paleogene sediments of the tropical Pacific have been compiled and put on the biostratigraphic and paleomagnetic timescale refined by ODP Leg 199 scientists. Sediment accumulation rates have been calculated for ten intervals ranging in age from 10 to 56 Ma and have been plotted for the midpoint of each interval at the associated paleoposition for each site used. A fixed hot spot model was used for reconstruction of the Pacific lithospheric plate. All such reconstructed intervals show the development of a tongue of high accumulation rates associated with the oceanographic divergence at the geographic equator. The development of this equatorial band is weakest between 46 and 56 Ma, the time of the peak warmth in Paleogene climate. Possible motion of the Hawaiian hot spot or true polar wander between 46 and 56 Ma appears to have had little effect on the plate rotation estimate of the position of the equator. In addition to temporal changes in the calcite compensation depth and in productivity, the biggest change in the patterns of sediment accumulation rates in the eastern tropical Pacific was the development of a relatively strong divergence between 6° and 10°N, near the region of divergence between the modern North Equatorial Current and the North Equatorial Counter Current. Changes in the equatorial circulation appear to be associated in time with the opening and closing of oceanic gateways, particularly the complex closing of the Caribbean-Pacific gateway. *INDEX TERMS:* 1525 Geomagnetism and Paleomagnetism: Paleomagnetism applied to tectonics (regional, global); 4231 Oceanography: General: Equatorial oceanography; 4263 Oceanography: General: Ocean prediction; 4279 Oceanography: General: Upwelling and convergences; *KEYWORDS:* equatorial Pacific, Cenozoic, Ocean Drilling Project

Citation: Moore, T. C., Jr., J. Backman, I. Raffi, C. Nigrini, A. Sanfilippo, H. Pälike, and M. Lyle (2004), Paleogene tropical Pacific: Clues to circulation, productivity, and plate motion, *Paleoceanography*, *19*, PA3013, doi:10.1029/2003PA000998.

1. Introduction

[2] The sediments of the tropical Pacific Ocean are dominated by a mound of biogenic sediments generated by high productivity associated with the equatorial divergence [*Ewing et al.*, 1968]. The Pacific Basin is unique not only in its great size, but also because the northward component of the Pacific Plate motion carries sediments generated in the equatorial zone gradually northward. Sedimentary deposits are eventually carried into regions of the North Pacific where productivity is low and sediment delivery to the ocean floor is very slow. As a result, a relatively broad equatorial mound of sediment has been built up over tens of millions of years, with its thickest part somewhat north of the equator. Another result of this northward movement of the Plate into regions of low sediment delivery is that older Cenozoic sediments are not deeply buried on the northern flank of the mound. These biogenic sediments tend to be relatively well preserved and are accessible using the Advanced Piston Coring (APC) techniques of the Ocean Drilling Program.

[3] By the 1970s the Deep Sea Drilling Project had drilled 24 sites into Cenozoic sediments of the Pacific equatorial mound. *van Andel et al.* [1975] summarized the findings from these sites, making a major contribution toward our understanding of the temporal and spatial changes in the rates and patterns of biogenic sedimentation in the equatorial Pacific. When corrected for changes in the biostratigraphy and chronostratigraphy that have occurred since 1975, the maxima in lower Neogene and Paleogene biogenic sediment accumulation appear between 22 Ma and 32 Ma. There is also an indication of high accumulation rates in the middle Eocene; however, the data were too sparse to clearly define this feature.

[4] In addition to changes in the rates at which biogenic sediments accumulated, *van Andel et al.* [1975] looked at the spatial patterns of sediment accumulation rates and interpreted them in terms of changes in upwelling intensity, changes in the preservation of carbonate, and erosional removal of sediments by bottom flow. *van Andel et al.*

[1]Department of Geological Sciences, University of Michigan, Ann Arbor, Michigan, USA.
[2]Department of Geology and Geochemistry, Stockholm University, Stockholm, Sweden.
[3]Dipartimento di Scienze della Terra, Universita G. D'Annuzio, Campus Univeritario, Chieti Scalo, Italy.
[4]Scripps Institution of Oceanography, University of California, San Diego, La Jolla, California, USA.
[5]Center for Geophysical Investigation for the Shallow Subsurface, Boise State University, Boise, Idaho, USA.

0883-8305/04/2003PA000998

[1975] and *Heath et al.* [1977] also documented major changes in the Carbonate Compensation Depth (CCD) through time. Over the Cenozoic the CCD has had a profound effect on the preservation of carbonate microfossils. The very shallow CCD during the early Paleogene nearly eliminated Pacific equatorial carbonate deposition except in regions shoaler than about 3300 m. The sharp drop in the CCD at the Eocene/Oligocene boundary and its gradual rise in the Miocene strongly influenced both the pattern and rates of biogenic sediment accumulation.

[5] Finally, *van Andel et al.* [1975] used their maps of equatorial sediment accumulation to define the location of the geographic equator through time. This allowed them to develop a model of plate rotation that was completely independent of the location of the paleomagnetic pole and of any assumptions regarding fixed "hot spots" or true polar wander. Although this model was constrained by the relatively few DSDP sites from which the sediment accumulation maps were made, it does compare well with the more modern plate rotation models used by the ODP Leg 138 study of the late Neogene Pacific equatorial zone [*Mayer et al.*, 1992; *Pisias et al.*, 1995].

[6] ODP Leg 199 returned to the equatorial Pacific to look at the Paleogene part of the record some 25 years after the *van Andel et al.* [1975] synthesis. During these years there had been more than 50 new sites drilled in the tropical Pacific. However, Leg 199 was the first ODP leg planned as an equatorial transect along the 56 Ma crustal isochron with a focus on the Eocene, a part of the section rarely well recovered and rarely containing carbonate fossils. This part of the equatorial section was inadequately recovered in the days of DSDP because of technical shortcomings in the drilling and coring systems in use at that time.

[7] In this paper we combine the results from the 8 sites drilled on ODP Leg 199 with 55 other sites that recovered Paleogene and lower Neogene sections. We use these data to develop an expanded synthesis of the regional depositional patterns in the tropical Pacific Ocean. In so doing we aim to verify the patterns described by *van Andel et al.* [1975]; expand coverage back through the Eocene; gain insights into the early Paleogene changes in circulation and depositional patterns; and establish the location of the geographic equator through time.

2. Methods

[8] One of the key elements in this synthesis is the use of a common stratigraphy and timescale. Although improvements to the Cenozoic timescale continue to be made, we have chosen to use the geomagnetic polarity timescale of *Cande and Kent* [1995], as amended by *Shackleton et al.* [1999]. The work by scientists on ODP Leg 199 has done much to make the task of stratigraphic synthesis easier [*Lyle et al.*, 2002]. First, the excellent paleomagnetic data recovered from the Leg 199 cores [*Lyle et al.*, 2002] allowed further refinement of several nannofossil datums around the Paleocene/Eocene boundary (Table 1). It also helped establish a reliable timescale for the Paleogene radiolarian stratigraphy (Table 2). The age of the radiolarian zone boundaries in Table 2 are an average of the estimated ages for six of the ODP Leg 199 sites that contained both good magnetic data and good preservation and recovery of siliceous sediments. This was critical for the Eocene sections because time control for this part of the section (which is usually free of carbonate) was virtually lacking in the earlier ODP and DSDP sites from this region. Paleomagnetic data were rarely available from the older cores taken in the region, but were used when available.

Table 1. Nannofossil Marker Species and Estimated Ages as Reported in the Work of *Lyle et al.* [2002][a]

Marker Species	Age, Ma
B_Discoaster neohamatus	10.45
B_Discoaster hamatus	10.48
B_Catinaster coalitus	10.8
T_(C) Discoaster kugleri	11.6
B_(C)Discoaster kugleri	11.9
T_Cyclicargolithus floridanus	13.3
T_Sphenolithus heteromorphus	13.55
B_Sphenolithus heteromorphus	17.7
T_Sphenolithus belemnos	17.94
T_Triquetrorhabdulus carinatus	19.6
B_Sphenolithus belemnos	18.9
B_Discoaster druggii	23.2
T_Sphenolithus delphix	22.98
B_Sphenolithus delphix	23.24
T_Sphenolithus ciperoensis	24.14
T_Sphenolithus distentus	26.3
B_Sphenolithus ciperoensis	26.9
T_Sphenolithus pseudoradians	29.1
B_Sphenolithus distentus	29.4
T_Reticulofenestra umbilicus $\geq$14μm	32.3
T_Ericsonia formosa	33
T_Discoaster barbadiensis	34.2
T_Discoaster saipanensis	34.4
T-Cribrocentrum reticulatum	34.9
T_Chiasmolithus grandis	37.1
B_Dictyococcites bisectus	38.5
T_Chiasmolithus solitus	40.4
B_Reticulofenestra umbilicus $\geq$14μm	42.5
T Chiasmolithus gigas	44
B_Chiasmolithus gigas	46.1
B_Nannotetrina fulgens	47
B_Nannotetrina spp.	47.8
T_Discoaster lodoensis	48
B_Discoaster lodoensis	52.4
T_Discoaster multiradiatus	53
B_Sphenolithus radians	53.3
B_Discoaster diastypus	53.9
B_Discoaster multiradiatus	56.2
B_Discoaster mohleri	57.5
B_Heliolithus kleinpellii	58.2
B_Fasciculithus tympaniformis	59.7

[a]Here B, base of species range; T, top of species range.

[9] One of the great successes of Leg 199 was the recovery of a high-resolution ($\sim$10–20 m/Myr) biogenic sediment record from the late Paleocene to the early Miocene. These sediments were found to contain an uninterrupted set of geomagnetic chrons, as well as a detailed record of calcareous and siliceous biostratigraphic datum points. In addition, lithological measurements revealed clearly recognizable cycles that can be attributed to climatic change, driven by Milankovitch style orbital variations of Earth. A synthesis of lithological proxy data (magnetic susceptibility, color reflectance, bulk density, per cent carbonate, XRF elemental measurements) and stable isotope measurements from Sites 1218 and 1219 allowed

Table 2. Radiolarian Zonal Boundaries and Estimated Ages Derived From ODP Leg 199 Studies[a]

Zonal Bounds	Marker Species	Age, Ma
RN7/6	D. petterssoni → D. hughesi	7.632
RN6/5	B_Diartus petterssoni	12.464
RN5/4	Dorcadospyris dentata → D. alata	15.453
RN4/3	B_Calocycletta costata	17.515
RN3/2	B_Stichocorys wolffii	18.853
RN2/1	T_Theocyrtis annosa	21.562
RN1/RP22	B_Cyrtocapsella tetrapera	22.589
RP22/21	B_Lychnocanoma elongata	24.869
RP21/20	T. triceros → D. ateuchus	29.001
RP20/19	Lithocyclia aristotelis → L. angusta	33.468
RP19/18	T_Thyrsocyrtis tetracantha (acme)	35.314
RP18/17	B_Calocyclas bandyca	36.723
RP17/16	B_Cryptocarpium azyx	37.59
RP16/15	B_Podocyrtis (L.) goetheana	40.067
RP15/14	Podocyrtis (L.)mitra → P. chalara	41.376
RP14/13	Podocyrtis (L.)sinuosa → P. mitra	43.27
RP13/12	Podocyrtis (P.)phyxis → P. ampla	44.519
RP12/11	B_Eusyringium lagena	46.165
RP11/10	B_Dictyoprora mongolfieri	49.021
RP10/9	Theocotyle nigriniae → T. cryptocephala	-
RP9/8	B_Theocorys anaclasta	-
RP8/7	Pterocodon? anteclinata → Buryella clinata	51.932

[a]From *Lyle et al.* [2002]. Here B, base of species range; T, top of species range; arrows show evolutionary transition.

a detailed comparison of these sites, as well as the correlation of nearby piston cores with comparable data. The integration of these sections into a single stratigraphy permitted relatively tight chronostratigraphic control on the biostratigraphy.

[10] The stratigraphies developed by many different DSDP and ODP workers and reported in the DSDP and ODP Leg Volumes were used in the synthesis process. Over recent decades nannofossil biostratigraphic datums have proven to be very reliable chronostratigraphic markers when checked against paleomagnetic data. By comparison radiolarian datums are only just beginning to be well calibrated to the magnetic timescale, particularly in the older part of the Cenozoic. If there ever appeared to be conflict between the radiolarian and nannofossil datums and age estimates, the nannofossil datums (Table 1) were used.

[11] Accumulation rates were calculated using meters below seafloor (mbsf) for the older sites and meters composite depth (mcd) where such data are available. Mcd depths tend to be a bit deeper (by 5–15%) than mbsf depths, but better represent the complete stratigraphic section. Thus the rates determined using mcd measures may be slightly higher than those using mbsf; however, such small differences in depth determination will have little effect on the regional patterns of long-term average accumulation rates presented here.

[12] We calculated average accumulation rates for 10 time intervals, each of 4–6 million years duration. In many cases several biostratigraphic datums were identified within each interval. However, in a few of the sites used, stratigraphic data were almost totally absent. In such cases very long term average accumulation rates were calculated and used in the maps. These tended to be sparsely fossiliferous ''red clay'' sections, but they were important to include in the synthesis for they serve to separate the areas where the biogenic component of sediments was significant from those where it was not. In several sites there is a clear biostratigraphic indication of missing section. If the section missing was less than the total duration of the averaged interval it served merely to lower the average accumulation rate. If the hiatus was greater than the interval averaged, a ''zero'' accumulation rate is reported for that interval.

[13] All the sites used in this study are located on the Pacific lithospheric plate during the Cenozoic (Figure 1). In this study we used the plate rotation schemes of *Engebretson et al.* [1985] and *Gripp and Gordon* [1990] to move sites to their estimated position at the middle of each averaged time interval. The speed of plate movement during the time span studied is about 0.2° to 0.25° per million years; thus, during a 4 Myr interval the sites have moved only about 100 km. This, then, is the approximate spatial resolution of our ''snapshot'' of sediment accumulation patterns. We have also made some alterations to the lateral boundaries of the tropical Pacific. Specifically, we have shifted the Australian, North American, and South American Plates with time and have opened the Straits of Panama, in accordance with the reconstructions available using the magnetic pole reference frame at the ODSN Web site (http://www.odsn.de/odsn/services/paleomap/paleomap.html) [*Hay et al.*, 1999]. As shown in our maps, these shifts in landmasses are only approximate, but they do give important insights into the impacts that the tropical ''gateways'' may have had on tropical Pacific surface circulation.

[14] The use of a ''fixed hot spot'' plate rotation model for Eocene and older times is controversial. Several lines of evidence indicate that between about 43 Ma and 80 Ma, the Hawaiian hot spot was not fixed [*Tarduno et al.*, 2003, 2002; *Christensen*, 1998; *Tarduno and Cottrell*, 1997; *Steinberger*, 1996; *Tarduno and Gee*, 1995; *Acton and Gordon*, 1994; *Petronotis et al.*, 1994; *Duncan and Richards*, 1991; *Sager and Pringle*, 1988; *Molnar and Stock*, 1987; *Sager and Bleil*, 1987; *Gordon*, 1983; *Kono*, 1980]. However, many questions remain: Are plate motion and hot spot motion necessarily linked? Did the

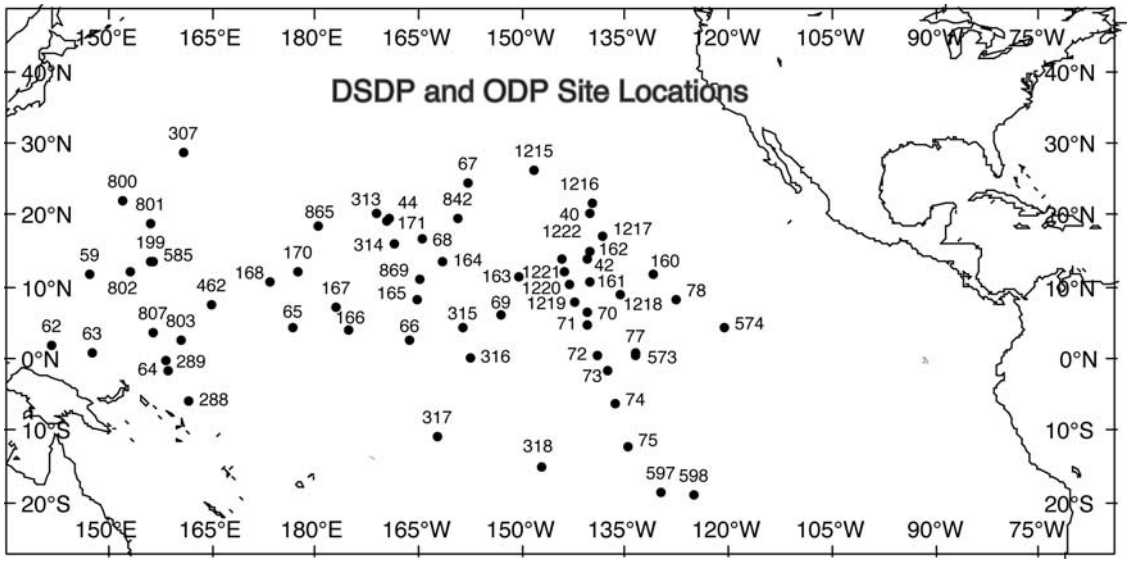

Figure 1. DSDP and ODP sites used in the reconstruction of average lower Neogene and Paleogene sediment accumulation rates. Filled circles indicate site locations associated with site numbers.

plate motion alter as the hot spot began to drift? Was there true wandering of either the geographic pole or the magnetic pole associated with the movement of the Hawaiian hot spot? We trace the location of the geographic pole through time by identifying the narrow zone of high rates of biogenic sedimentation that is associated with the equatorial divergence, a divergence caused by the change in the sign of the Coriolis effect at the geographic equator. In contouring the accumulation rate values, we were influenced by the zonal pattern of modern accumulation rates and the sharp drop off in these rates north and south of the equator. In nearly all the maps the equatorial tongue of higher accumulation is readily identified and tightly constrained (Figures 2–11). We have identified the position of the geographic equator as the center of this tongue, fitting its position by eye to pass through the center of the tongue and through the center of the patch of higher accumulation rates in the extreme western equatorial Pacific. In the modern ocean the major impact of this divergence band is only a couple of degrees of latitude in width. Even with additional uncertainty resulting from the use of 4 to 6 Myr averages of accumulation rates, we should be able (with sufficient site coverage) to locate the geographic equator to within ±1°. This is considerably better than the accuracy in the location of paleomagnetic poles through time. To the extent we are able to identify clearly this oceanographic feature in the Eocene maps, we can contribute to a better understanding of how much hot spot movement and/or true polar wander could have affected the reconstruction of the Pacific Plate position during this time interval.

3. Results

[15] All the sites used in these reconstructions are shown in Figure 1. These include all the sites drilled in the tropical Pacific prior to ODP Leg 199 that contained adequate recovery and stratigraphic information for lower Neogene and Paleogene sections. As we step back in time through the subsequent figures, the relative positions of the sites should not change; however, their positions do move to the ESE relative to the plate boundaries.

[16] The mapped sediment accumulation rates of the middle Miocene (10–14 million years ago (Ma) (Figure 2) show a pattern typical of much of the Holocene through Neogene. There is a relatively narrow tongue (about 5° of latitude in width) of biogenic silica and carbonate that accumulated at rates greater than 10 m/Myr and with peak rates between 20 and 25 m/Myr.

[17] There are several sites on this and following maps that owe their higher accumulation rates to relatively shallow water depths at the site locations, which results in good preservation of carbonate. These include two sites south of the equator, located at ~2600 m on the Manihiki Plateau (Site 317) and within the Tuamotu Island chain (Site 318). Similarly, in the west the shallow sites located on and near the Ontong Java Plateau have well preserved carbonate sections and higher accumulation rates. In addition, between the Ontong Java Plateau and the equatorial tongue of high accumulation rates, Site 167 is located on the Magellan Rise at ~3200 m and has accumulation rates distinctly higher than surrounding sites.

[18] The next older "snapshot" (Figure 3) of the lower middle Miocene has a pattern nearly identical to that of the upper middle Miocene (cf. Figures 2 and 3). The main difference is that maximum accumulation rates in the equatorial zone are somewhat higher than in the younger interval. The zone of rates >5 m/Myr also extends about 10° of longitude farther west in the older section.

[19] In the 18–22 Ma "snapshot" (Figure 4), accumulation rates are somewhat lower. However, the Magellan Rise Site (167) and nearby Sites 65 and 166 all show increased accumulation rates as they are rotated closer to the equator. As we go back into the upper Oligocene (Figure 5; 22–26 Ma) the area to the south of the equator

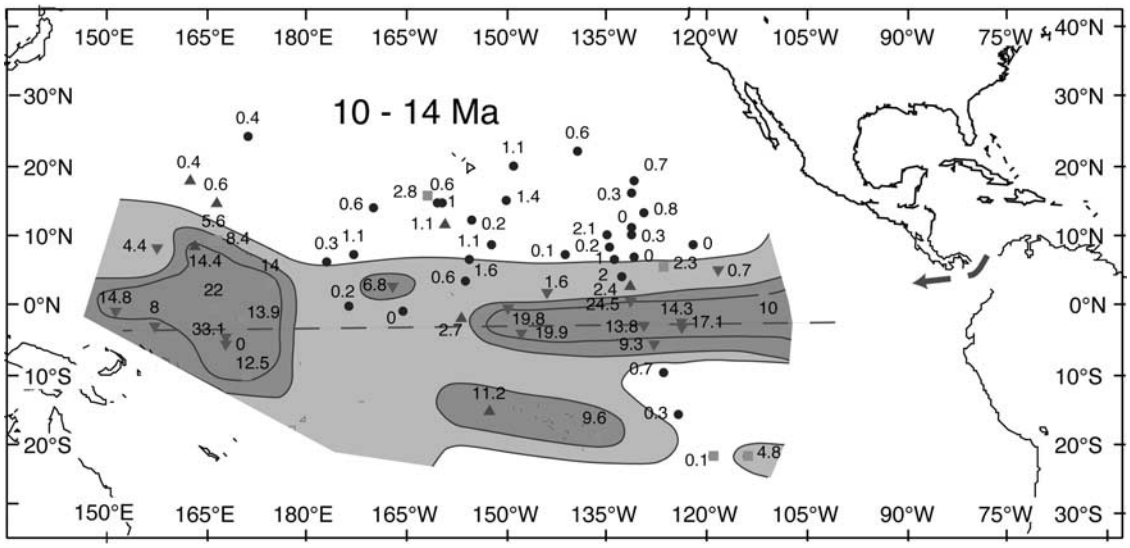

Figure 2. Average sediment accumulation rates for the interval 10–14 Ma given in units of meters per million years. Site positions are rotated to their estimated position at 12 Ma [*Engebretson et al.*, 1985; *Gripp and Gordon*, 1990]. Site location are marked and colored according to the microfossils used in the biostratigraphic reports for the time interval: filled squares (blue) show carbonate microfossils, inverted filled triangles (green) show siliceous and carbonate microfossils, filled triangles (red) show siliceous microfossils, and filled circles (brown) show clay or sparse siliceous microfossils. A red dashed line marks the approximate center of the equatorial divergence (geographic equator). Contours are at 1, 5, and 10 m/Myr. See color version of this figure at back of this issue.

with accumulation rates higher than 5 m/Myr is broader than in younger intervals. This is a time when the CCD is deep [*Heath et al.*, 1977], and the Magellan Rise and the relatively shallow Ontong Java Plateau still lie within the equatorial zone of high productivity. The northern boundary of the equatorial zone remains sharp, with biogenic oozes rapidly giving way to red clays within 7° of the equator. However, as the sites are backtracked to more eastern longitudes there is an accompanying broadening of the zone of high accumulation rates in the extreme eastern equatorial Pacific that may be associated with eastern and western boundary currents as well as flow from the Caribbean.

[20] The mid part of the Oligocene looks very different (Figure 6; 26–30 Ma). The equatorial tongue of high

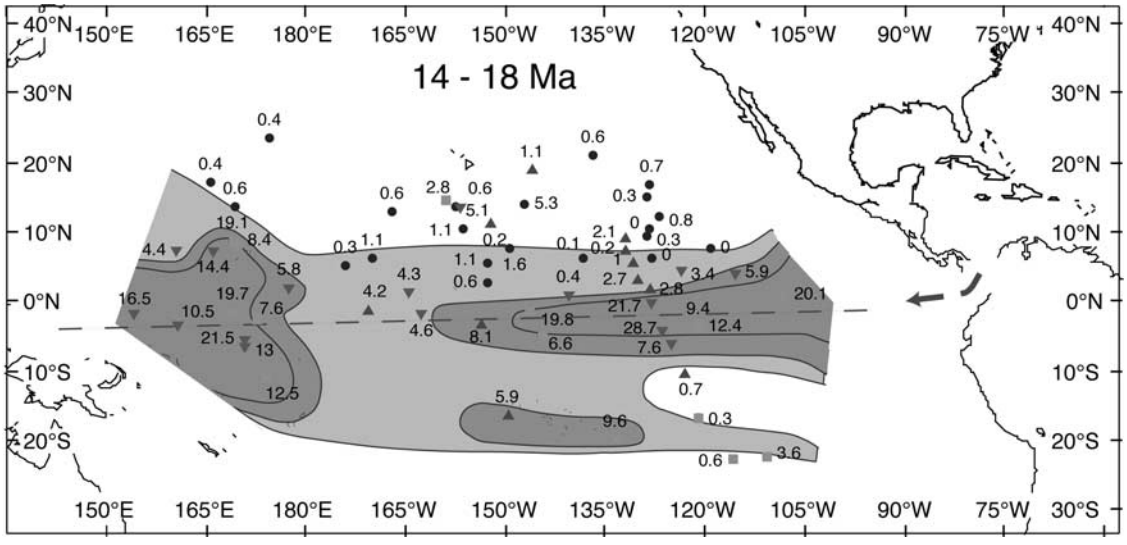

Figure 3. Average sediment accumulation rates for the interval 14–18 Ma given in m/Myr. Site positions are rotated to their estimated position at 16 Ma. Site location symbols and colors according to biostratigraphies used for the time interval. Symbols, colors, contours, and dashed line are as given in the caption to Figure 2. See color version of this figure at back of this issue.

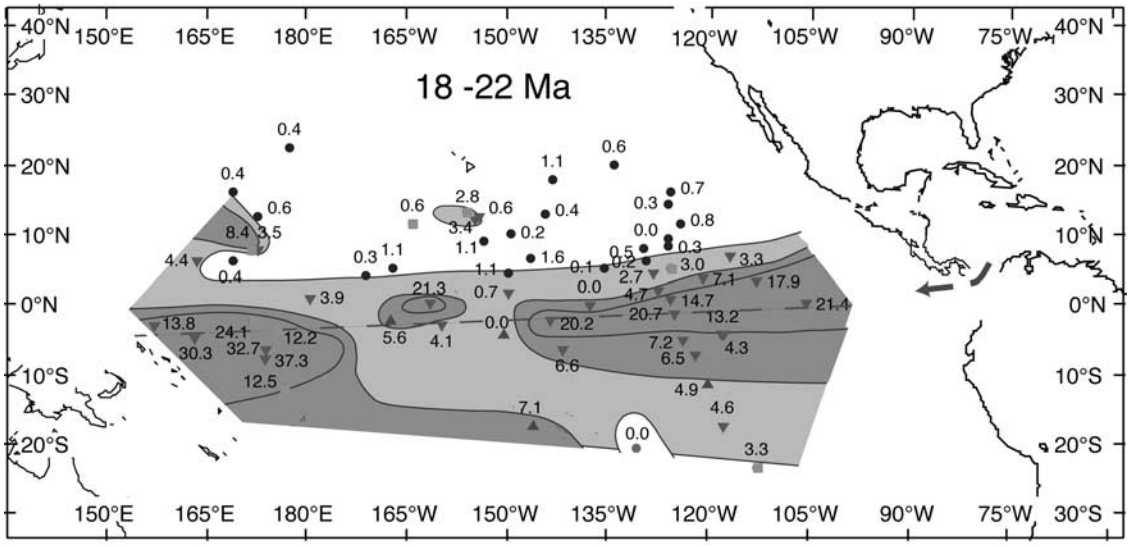

Figure 4. Average sediment accumulation rates for the interval 18–22 Ma given in m/Myr. Site positions are rotated to their estimated position at 20 Ma. Site location symbols and colors according to biostratigraphies used for the time interval. Symbols, colors, contours, and dashed line are as given in the caption to Figure 2. See color version of this figure at back of this issue.

accumulation stretches across the shallow rises and appears to broaden greatly in the eastern tropical Pacific. Even though the equatorial divergence zone is easily recognizable, there are maxima in accumulation rates located on either side of the equator that are as high as values associated with the equatorial divergence. This feature argues for strong advective flow of nutrient rich waters into the region, particularly from the south. To the north, Site 171, located several degrees north of the equator (at about 10°N, 148°W paleoposition) also has an anomalously high rate of over 10 m/Myr. The presence of high values in this one North Pacific site might be taken as a stratigraphic "outlier," except for the fact that as we go farther back in time, a narrow northern zone of high accumulation rates becomes quite distinct between about 6°–10° north of the equatorial tongue. This is seen in both the lower Oligocene snapshot (Figure 7; 30–34 Ma) and the upper Eocene (Figure 8; 34–40 Ma). An additional difference in these latter three reconstructions (Figures 6–8) is the apparent development of a broad zone (or tongue) of higher

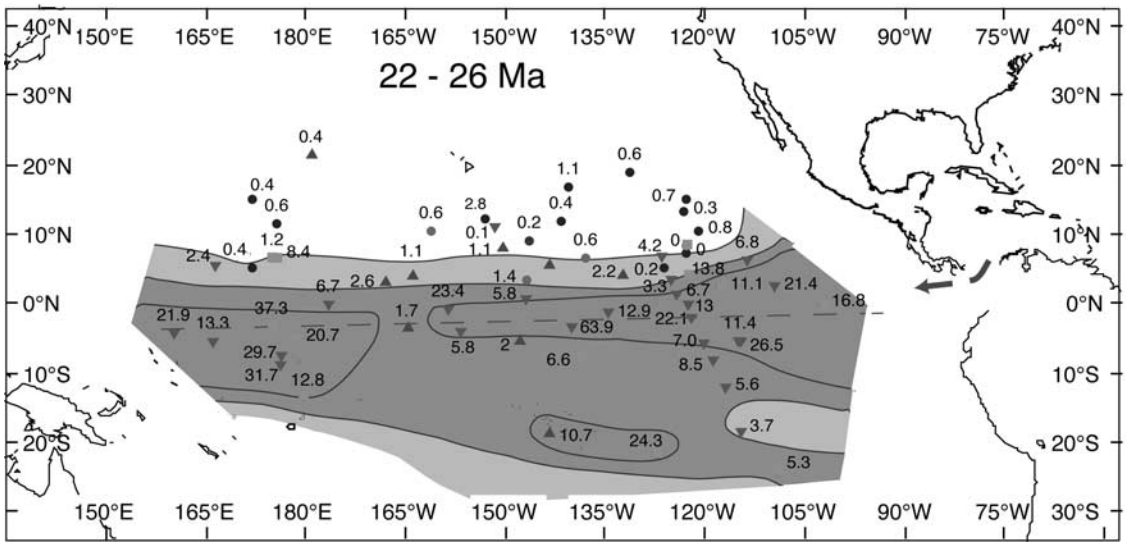

Figure 5. Average sediment accumulation rates for the interval 22–26 Ma given in m/Myr. Site positions are rotated to their estimated position at 24 Ma. Site location symbols and colors according to biostratigraphies used for the time interval. Symbols, colors, contours, and dashed line are as given in the caption to Figure 2. See color version of this figure at back of this issue.

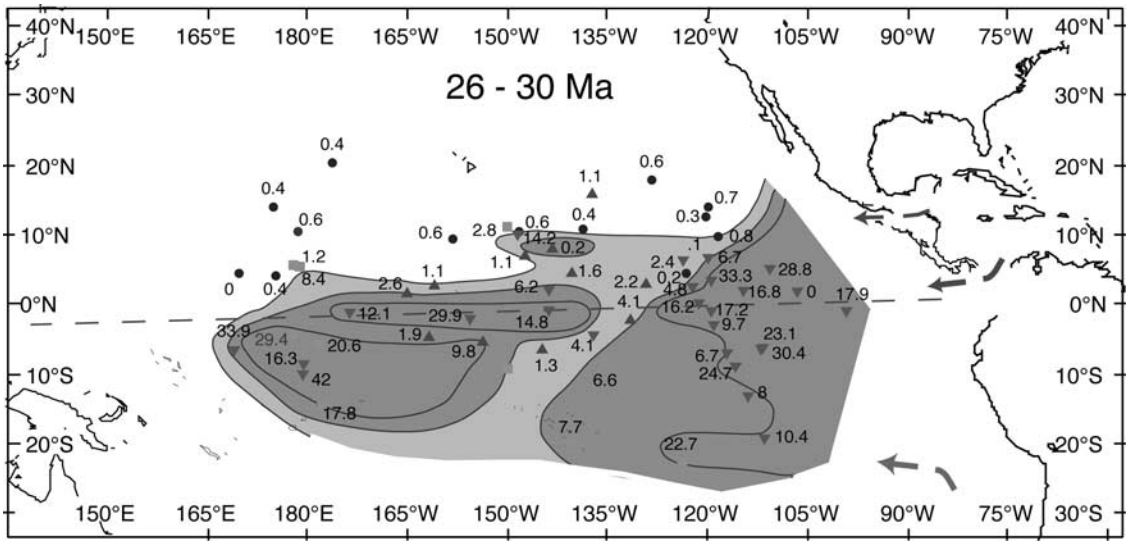

Figure 6. Average sediment accumulation rates for the interval 26–30 Ma given in m/Myr. Site positions are rotated to their estimated position at 28 Ma. Site location symbols and colors according to biostratigraphies used for the time interval. Symbols, colors, contours, and dashed line are as given in the caption to Figure 2. See color version of this figure at back of this issue.

accumulation rates in the eastern South Pacific (~20°–30°S), although the presence of this feature is controlled by only a few sites.

[21] The CCD rapidly dropped some 1200 m at the upper Eocene-lower Oligocene boundary [*Heath et al.*, 1977; *Lyle et al.*, 2002], and carbonate deposition is virtually absent from Pacific sites deeper than 3300 m in the "predrop," shallow-CCD Eocene. However, the lower Oligocene and upper Eocene patterns of sediment accumulation are nearly identical (cf. Figures 7 and 8). This strongly argues for the factors controlling the patterns of accumulation rates in these two snapshots being wind driven surface circulation and boundary conditions rather than preservation of carbonate sediments.

[22] Approximately the same pattern is seen in the upper middle Eocene as well (Figure 9; 40–46 Ma) and differs only in the somewhat higher average rates of accumulation in the extreme eastern equatorial Pacific. The lower middle Eocene (Figure 10; 46–50 Ma) also has this pattern; however the overall rates of accumulation are much lower. Accumulation rates in the few sites located in the southeastern corner of the reconstructions maintain values of 10–

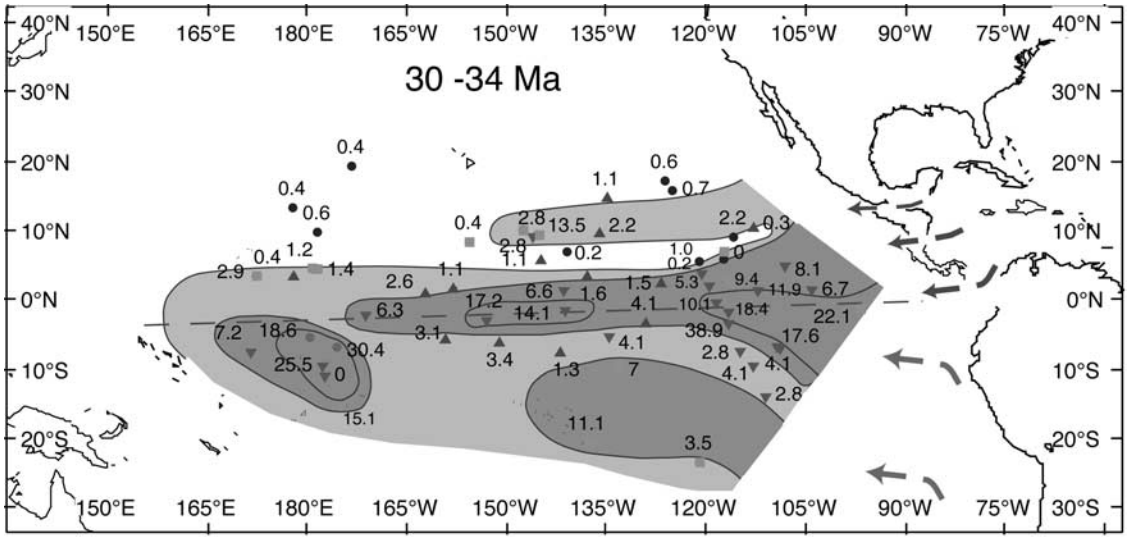

Figure 7. Average sediment accumulation rates for the interval 30–34 Ma given in m/Myr. Site positions are rotated to their estimated position at 32 Ma. Site location symbols and colors according to biostratigraphies used for the time interval. Symbols, colors, contours, and dashed line are as given in the caption to Figure 2. See color version of this figure at back of this issue.

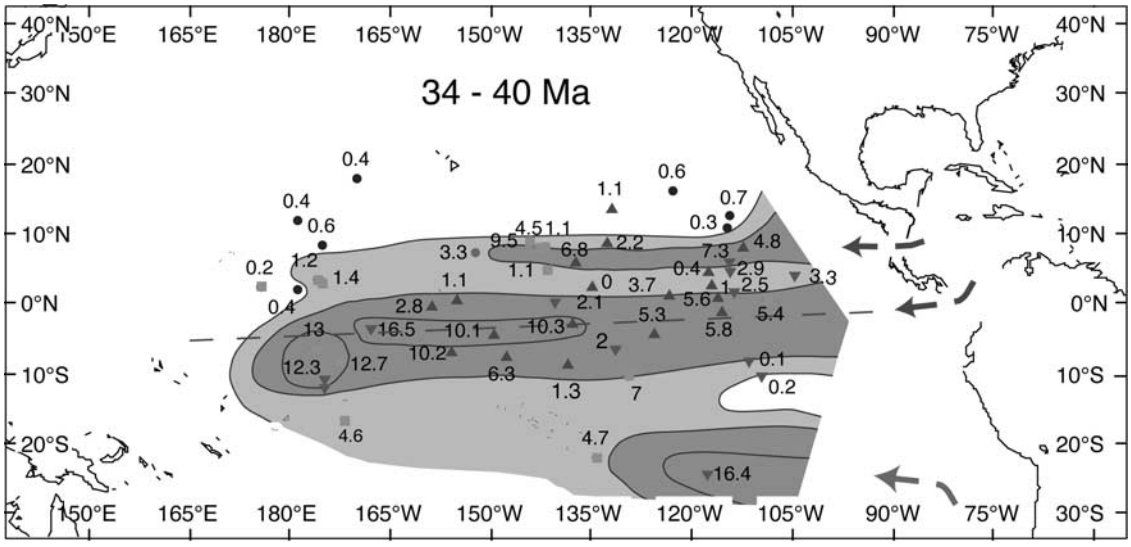

Figure 8. Average sediment accumulation rates for the interval 34–40 Ma given in m/Myr. Site positions are rotated to their estimated position at 37 Ma. Site location symbols and colors according to biostratigraphies used for the time interval. Symbols, colors, contours, and dashed line are as given in the caption to Figure 2. See color version of this figure at back of this issue.

20 m/Myr throughout the upper and middle Eocene (Figures 8–10).

[23] By the time we reach back to the lower Eocene (Figure 11; 50–56 Ma), the number of sites that can be used to constrain the accumulation rate pattern is much reduced. It is more difficult to unambiguously delineate the equatorial tongue, whereas to the north and south of the equator there is good evidence for relatively high accumulation rates. Accumulation rates in the northeastern tropical Pacific are consistently high relative to most of the other sites containing lower Eocene sediments.

[24] In Figures 2–11 the equatorial tongue of high accumulation rates is recognizable and nearly always extends westward to at least 160°W paleolongitude. However, it appears that the geographic equator as defined by this tongue is offset to the south and somewhat tilted relative to the ''reconstructed'' paleoequator defined by the plate rotation scheme. Our best estimate of the position of the geographic paleoequator is indicated by a dashed line in Figures 2–11. We use this estimated position of the equator for each time interval to recalculate the paleolatitude of the eastern equatorial Pacific sites that best define

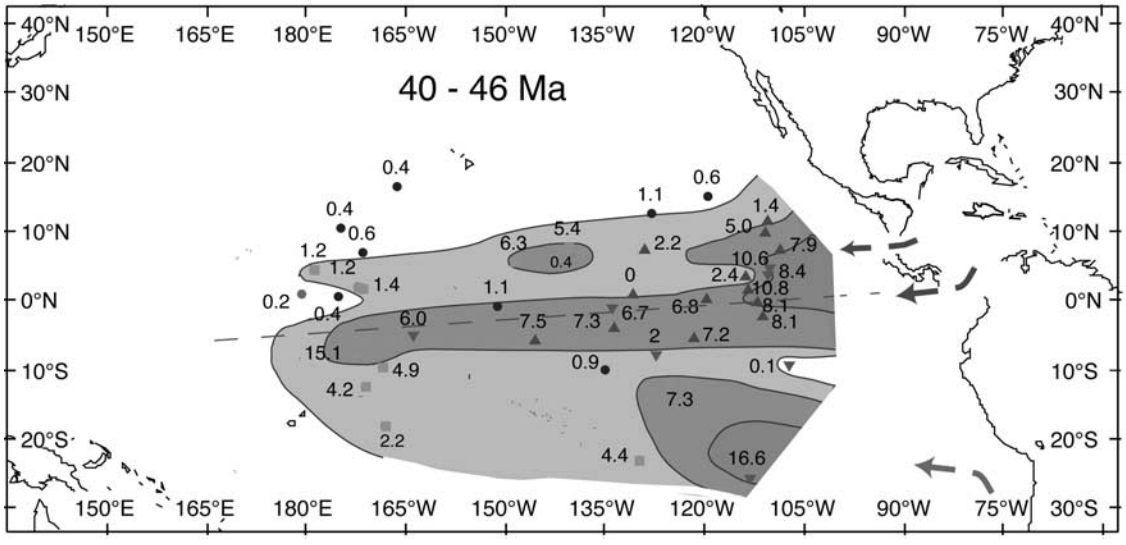

Figure 9. Average sediment accumulation rates for the interval 40–46 Ma given in m/Myr. Site positions are rotated to their estimated position at 43 Ma. Site location symbols and colors according to biostratigraphies used for the time interval. Symbols, colors, contours, and dashed line are as given in the caption to Figure 2. See color version of this figure at back of this issue.

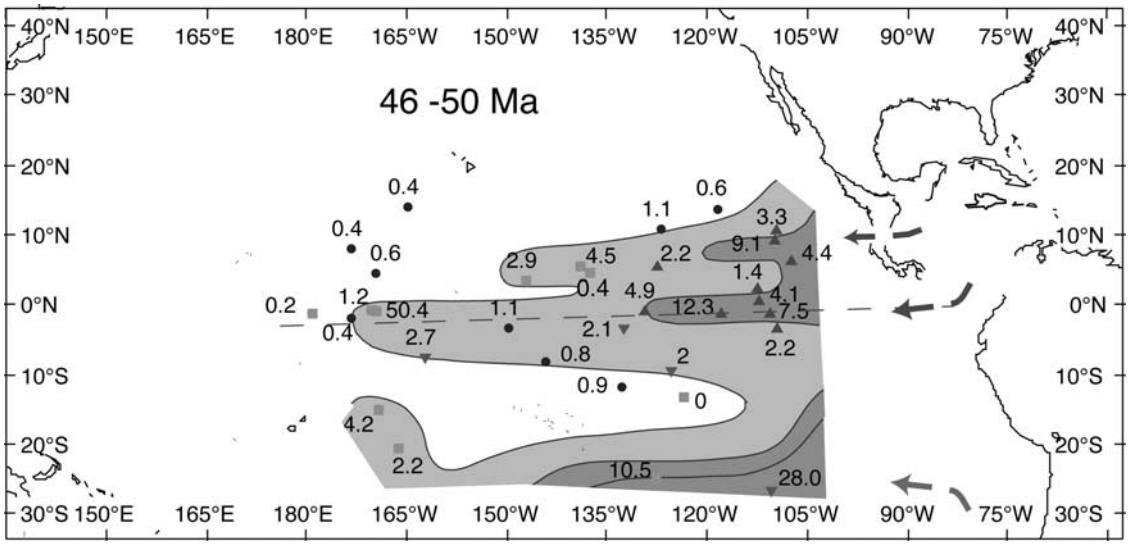

Figure 10. Average sediment accumulation rates for the interval 46–50 Ma given in m/Myr. Site positions are rotated to their estimated position at 48 Ma. Site location symbols and colors according to biostratigraphies used for the time interval. Symbols, colors, contours, and dashed line are as given in the caption to Figure 2. See color version of this figure at back of this issue.

this zone of divergence (i.e., those sites east of ~160° W paleolongitude) and produce "corrected " paleolatitudes for these sites. These eastern equatorial Pacific sites are plotted in a series of latitudinal transects (Figure 12) representing each of the reconstructed intervals. Although we have averaged over relatively broad time intervals, these transects clearly show: 1) the sharp drop off in accumulation rates 4°–6°north of the equator in reconstructions younger than 26 Ma (Figures 12a–12d), 2) the increased equatorial accumulation rates in the Oligocene at ~22–32 Ma (Figures 12d–12f) found by *van Andel et al.* [1975] (note the near doubling of the scale range of the "Y axis" in Figures 12d–12f that is necessary to accommodate sites with higher accumulation rates during these intervals), 3) the distinctly lower accumulation rates in the Eocene (Figures 12g–12j), 4) the development of higher accumulation rates in a zone north of the equator (Figures 12e–12j), and 5) some indication of higher accumulation rates to the south of the equator prior to about 28 Ma (Figures 12e–12j).

[25] In the modern ocean there is a secondary band of high productivity to the north of the equator associated with moderate divergence at the southern boundary of the North

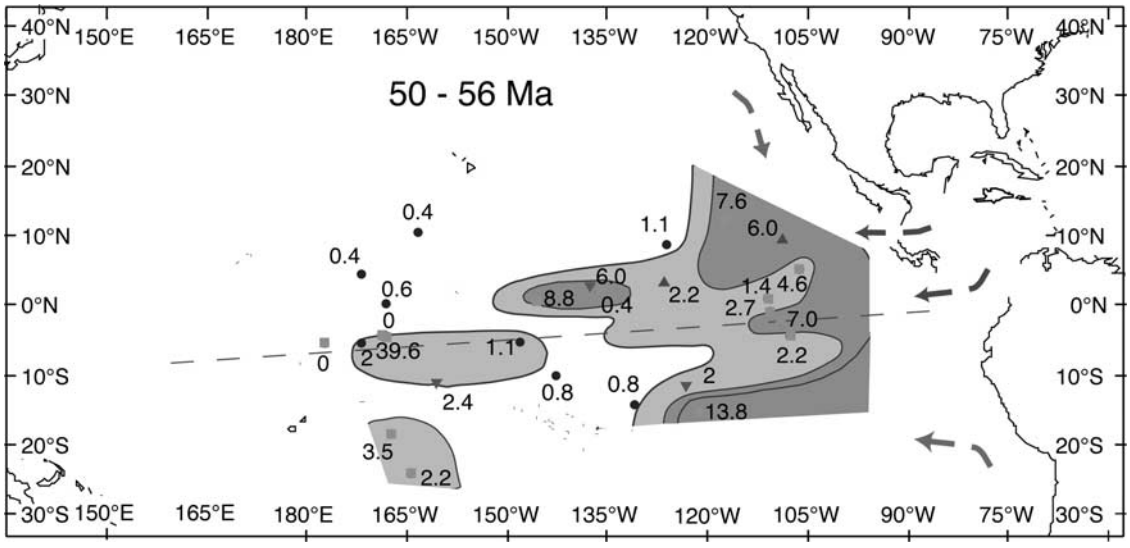

Figure 11. Average sediment accumulation rates for the interval 50–56 Ma given in m/Myr. Site positions are rotated to their estimated position at 53 Ma. Site location symbols and colors according to biostratigraphies used for the time interval. Symbols, colors, contours, and dashed line are as given in the caption to Figure 2. See color version of this figure at back of this issue.

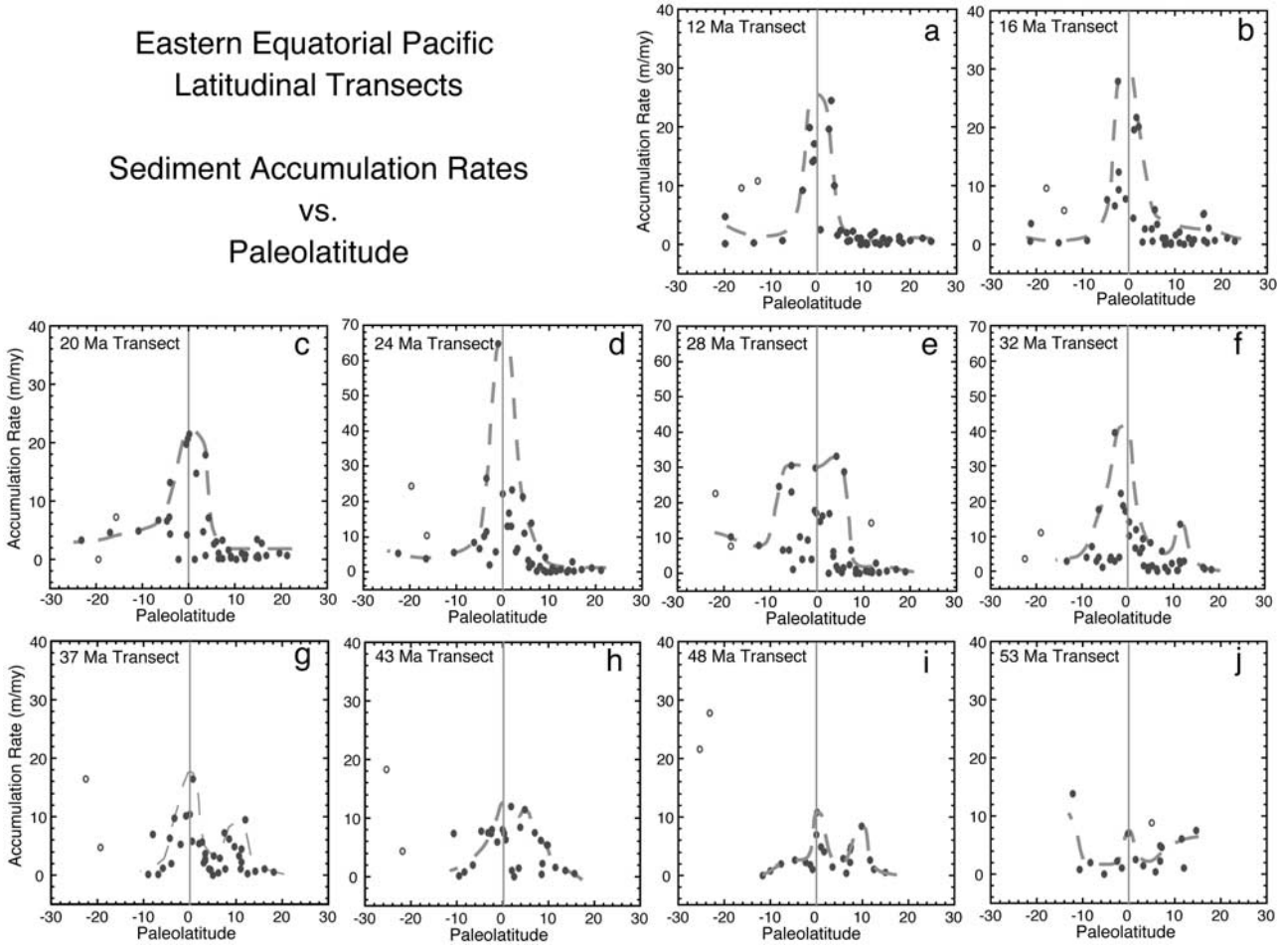

Figure 12. Sediment accumulation rates for sites east of 160°W paleolongitude plotted versus the site paleolatitude for each reconstructed time interval. Open circles indicate sites drilled at <3000 m water depths. Paleolatitudes are measured relative to the paleoequator as defined by the dashed line through the center of the equatorial zone of higher accumulation rates in Figures 2–11.The vertical line marks the estimated position of the maximum equatorial divergence (i.e., the "geographic equator"). The dashed line outlines the higher accumulation rates seen in each transect. On the basis of the paleolatitude of the sites in each reconstruction and on the averaging effect of accumulation rate estimations, the estimated position of the geographical equator could have an error of about ±1° of latitude. See color version of this figure at back of this issue.

Equatorial Current (NEC) where it meets the eastward flowing North Equatorial Counter Current (NECC). However, the impact of such increased productivity is rarely detected in Neogene and Quaternary sediments, nor is it seen in any of our younger reconstructions of sediment accumulation presented here (Figures 2–5 and 12a–12d). However, in the mid Oligocene and older reconstructions there is a broadening of the zone of high productivity in the eastern equatorial Pacific (Figures 6 and 12e) and the development of a narrow band of higher accumulation rates from about 6° to 10°N (corrected paleolatitude) in the older reconstructions (Figures 7–11 and 12f–12j). This band of higher rates approximates the position of the divergence at the boundary between the NEC and the NECC in the modern ocean.

[26] Figure 13 shows a summary of average (median) sediment accumulation rates in the eastern tropical Pacific through time. The median values of sediments accumulation rates in the equatorial zone (~4°S to ~4°N corrected paleolatitude) are plotted along with the median values of accumulation rates in the NEC/NECC zone (~6°N to ~10°N corrected paleolatitude). Both zones show peaks in accumulation rates at 22–26 Ma and at 40–46 Ma, intervals that have been identified previously as having relatively high accumulation rates of biogenic sediments in the equatorial Pacific [*van Andel et al.*, 1975]; *Moore et al.*, 2002a]. However, this plot also indicates that accumulation rates in the equatorial zone started with very low values in the lower and lower middle Eocene and then trended toward higher values in the middle Eocene, Oligocene and Miocene. It also shows relatively high rates in the northern (NEC/NECC) zone throughout the Eocene, dropping precipitously in the Oligocene. In the lower and lower middle Eocene the median rates in the northern zone are

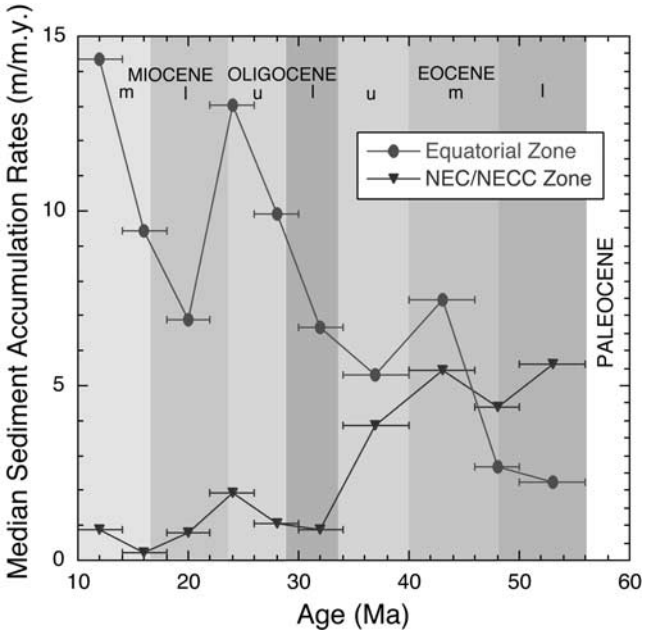

Figure 13. Median sediment accumulation rates for sites east of 160°W paleolongitude in the equatorial zone of high accumulation rates (~4°N–4°S; filled circles) and in the northern (NEC/NECC) zone (~6°–10°N; filled inverted triangles) for each of the ten reconstructed time intervals. Horizontal bars indicate length of each time interval over which accumulation rates are averaged. See color version of this figure at back of this issue.

about twice as high as those in the equatorial zone. This difference in relative sediment delivery rates in the two zones is consistent with results of modeling the early Eocene Pacific Ocean [*Huber*, 2002] that indicate more extensive divergence and a shoaler thermocline in the northern zone than along the equator.

[27] In his model results *Huber* [2002] shows strong divergence south of the equator as well, although he questions this feature as perhaps an artifact of the model itself. There are fewer data in the southern part of the study area against which to check these model results. The sediment accumulation rate data south of the equatorial zone include some sites that are comparatively shallow (<3000 m modern water depths, open symbols in Figure 12); and thus, were located above the CCD in the Eocene.

4. Discussion and Conclusions

4.1. Plate Rotation

[28] We have developed ten reconstructions of sediment accumulation rates in the tropical Pacific using a "fixed hot spot" model of Plate rotation. These maps allow us to compare how well the location of the "rotated" equator compares with an independent determination of the geographic equator, as defined by the location to the equatorial tongue of high productivity and high sediment accumulation rates. The two "equators" thus defined lie within a few degrees of each other in all the reconstructions. Given that the rotation rates and pole position both have errors associated with their estimation, and given that the definition of a geographic equator is based on a relatively few sites scattered in the tropical Pacific, we feel that this agreement is quite good. It does appear, however, that the geographic equator lies consistently south of the modeled equator and appears to be tilted to the southwest in nearly all the reconstructions. Slight adjustments to the plate rotation pole and speed might eliminate these differences.

[29] Although we have used a fixed hot spot rotation model to position the Pacific Plate and the sites studied through time, there is compelling evidence that the Hawaiian hot spot was not fixed and/or there was possibly some amount of true polar wander during the Cretaceous and early Cenozoic (until ~47 Ma [*Tarduno et al.*, 2003]). However, we cannot detect in our data any indication that the Pacific Plate was moving differently between about 56 and 46 Ma than it was after that time. There is a consistent offset between the modeled equator and the geographic equator of a little over 1° to the south (as measured at 120°W paleolongitude; Figure 14) that extends from the middle Miocene through the lower Eocene mapped intervals. Small changes in the amount of this offset may be associated with changes in the rotation speed or pole of rotation used in the rotation model (Figure 14). These results suggest that over the time interval studied true polar wander was very small (if it existed at all) and that hot spot motion was either small or not tightly coupled to movement of the lithospheric plate. It is unfortunate that our reconstructions do not reach farther back in time to provide a more extended comparison of apparent plate motion with the independent measurement of hot spot motion [*Tarduno et al.*, 2003].

4.2. Changes in Accumulation Rates

[30] *van Andel et al.* [1975] calculated accumulation rates averaged over one million year intervals and saw variation in these rates by factors of 5 to 10 through the Miocene and Oligocene. Peaks in accumulation rates usually lasted 2 to 3 my. Over the time interval studied here, sediment accumulation rates in the equatorial tongue of high productivity appear to have varied by at least a factor of 2 to 5. This is quite a large range considering that we are averaging over 4 to 6 Myr of time, which tends to smooth any larger, shorter-term variation. The lowest rates of equatorial sediment accumulation occur in the upper and lower Eocene intervals. The middle Eocene seems to have experienced a burst in productivity of organisms producing siliceous microfossils. In a more detailed look at Leg 199 results [*Moore et al.*, 2002a] there appear to have been two peaks in equatorial sediment accumulation within the 40–46 Ma interval, one at about 40.5 Ma and one at 44.5 Ma. The younger of these peaks appears to correlate with the sharp drop in high latitude temperatures following the middle Eocene climatic optimum (MEOC) identified by *Bohaty and Zachos* [2003]. The older middle Eocene peak in accumulation rates precedes the MEOC; however, oxygen isotope data in the 43–45 Ma interval are more sparse [*Bohaty and Zachos*, 2003], thus a comparison with high latitude climate cannot be made.

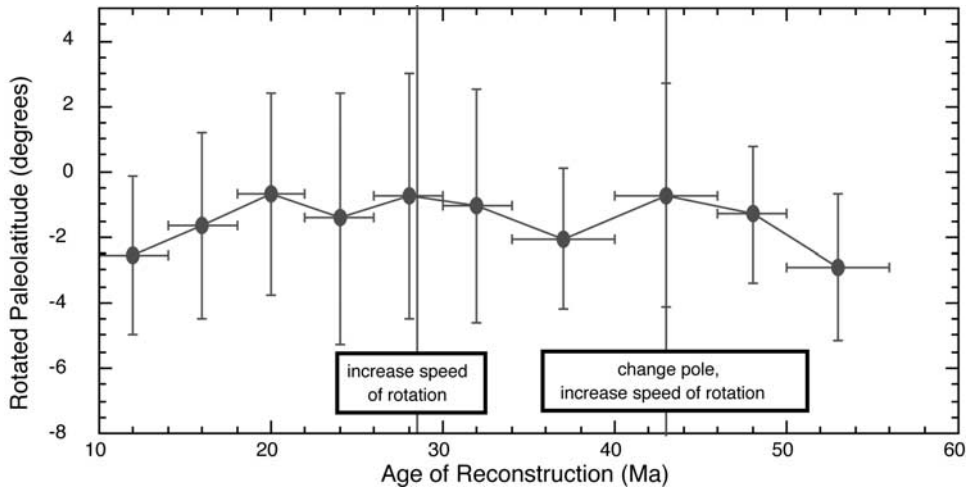

Figure 14. Rotated latitudinal position of geographic equator at 120°W paleolongitude. Geographic equator defined by equatorial zone of high accumulation rates and marked by dashed lines in Figures 2–11. Horizontal bars indicate length of each time interval over which accumulation rates are averaged. Vertical bar indicates width of equatorial zone of high accumulation rates. Vertical lines indicate times at which either the pole of rotation or angular speed of rotation changed in the rotation model [*Engebretson et al.*, 1985]. See color version of this figure at back of this issue.

[31] The depth of the CCD through time [*van Andel et al.*, 1975; *Heath et al.*, 1977] has a strong impact on the magnitude of sediment accumulation rates in the tropical Pacific. Certainly the shallow sites on the Ontong Java Plateau, the Magellan Rise, the Manihiki Plateau, and within the Tuamotu Islands have consistently higher accumulation rates than surrounding sites at greater depths. This is particularly true in the Eocene when the CCD was at 3200–3300 m, although it is possible that the CCD was somewhat deeper in the South Pacific and in the western tropical Pacific than it was in the North Pacific and eastern tropical Pacific. Even areas near these highs can have anonymously high rates through downslope transport of sediments (e.g., Site 199). At some sites on the very shallow parts of the Ontong Java Plateau (e.g., Site 289 at present-day water depth of 2206 m and corrected paleolatitude of 6°–12°S) long-term average rates dropped below 5 m/Myr in the middle and lower Eocene. Nearby Site 807(at present-day water depth of 2815 m) was much closer to the equator during the middle and late Eocene (2°S–4°S corrected paleolatitude). Long-term average Eocene rates are also lower than in the Oligocene at this site; however, much of this change in average rates is caused by the presence of numerous hiatuses in the Eocene section, hiatuses that are likely to have lowered average rates at Site 289 as well. Although the number of sites in the western tropical Pacific are not large there does seem to be a tendency for average accumulation rates in these sites to increase when they are close to the equator.

[32] If we focus strictly on the equatorial tongue of high accumulation rates in the eastern tropical Pacific (Figure 12), the highest values are found in the Oligocene and lowermost Miocene when the CCD was close to 5000 m deep [*van Andel et al.*, 1975]. These higher rates often reach peak values in the eastern tropical Pacific where the presence of both strong upwelling and advection of nutrient rich waters from the Peru-Chile Current contribute to higher productivity. In Miocene and older times the open passageway between South and Central America may have also contributed to increased divergence and higher productivity [*Huber and Sloan*, 2000].

[33] The westward extent of the equatorial tongue of high accumulation is more difficult to estimate because this measure is strongly influenced by the shallower sites of the western tropical Pacific as they drifted into and out of the equatorial band. However, it does appear that the westward extent of high equatorial accumulation rates was relatively small in the middle Miocene and in the lowermost Miocene and may have reached its greatest westward extent in the lower Oligocene (cf. Figures 4–9).

[34] It is a bit surprising that in the upper and upper middle Eocene (Figures 8 and 9), the westward extent of the equatorial tongue is just as great as in the lower Oligocene. This is true even though the CCD is much shallower and carbonate preservation is poor, and in spite of the fact that peak accumulation rates within the Eocene equatorial band are lower than in the Oligocene and younger sections (Figure 12). The westward extent of the equatorial band in the middle and upper Eocene is controlled by accumulation rates at Site 462 in the Nauru Basin. At a present depth of 5181 m, Site 462 still has siliceous and carbonate microfossils well back into the Eocene. This pattern indicates that equatorial upwelling induced by Trade Winds was a strong feature of the Eocene as suggested by the circulation models of *Huber* [2002] and *Huber and Caballero* [2003].

[35] The strength of equatorial upwelling appears to diminish markedly in the lower middle Eocene and lower Eocene (Figures 10–11). However, it does not disappear altogether as suggested by *Sun* [2000], *Liu and Huang*

[1997], and *Fedorov and Philander* [2000]. These two intervals span the peak in warmth of the early part of the Eocene [*Zachos et al.*, 1994, 2001]. Lower accumulation rates in both the lower middle Eocene (Figure 10) and lower Eocene (Figure 11) are affected by apparent hiatuses in the sections. The zonal boundary markers for the radiolarians are missing in all sites near ~50 Ma (Table 2), at the "climatic optimum" of the Eocene [*Zachos et al.*, 2001]. The poorly developed zone of equatorial high productivity during these two intervals (46–56 Ma) does suggest that the diminished pole to equator temperature gradient at this time had an impact on Trade Wind strength and the development of equatorial upwelling.

[36] Seen in the larger context of long-term changes in average accumulation rates of the eastern tropical Pacific (Figure 13), the most striking feature is the strength of the northern (NEC/NECC) zone of high accumulation rates during the Eocene. This is particularly true in the earlier part of the Eocene when accumulation rates associated with the equatorial divergence were at their lowest ebb. The strength of the northern zone of divergence as indicated by the accumulation rates is greatest during the Eocene and drops markedly in the Oligocene. The pattern of a separate NEC/NECC zone of higher accumulation rates, distinct from the equatorial zone, remains intact well into the Oligocene (cf. Figures 6–8). This is in spite of the large shift in climate from the late Eocene into the early Oligocene.

[37] Both the South Equatorial Current and the North Equatorial Current are trade wind–driven systems. The distinct difference in the evolution of the two zones of divergence associated with these currents suggests that we need to look to seasonal changes, changes in near-surface density distributions, and changes in the lateral boundaries of the Pacific basin if we are to explain the differences in accumulation rates associated with these divergences.

4.3. Changes in Circulation Patterns

[38] *Huber* [2002] in his model of the early Eocene Pacific shows a narrow zone having a relatively shallow thermocline (70 m) near 10°N associated with the NEC/NECC divergence. This zone extends farther west than that of the equatorial divergence itself and in this respect appears similar to the patterns of sediment accumulation seen for the lowermost Eocene (50–56 Ma; Figure 11). However, the zone of higher rates seen at 10°S that might match the southern shallow thermocline zone shown by *Huber* [2002] is not well defined; nor does the greater zonal extent of higher accumulation rates north of the equator persist into younger intervals. Part of the difficulty in making these comparisons may lie with the fact that there are fewer data points defining the depositional patterns of the early Eocene.

[39] In addition to the strength of the wind field and near-surface density structure, the lateral boundaries of the Pacific basin have a strong impact on the patterns of surface circulation. In our reconstructions, we have modified the two main tropical Pacific gateways to gain insight into how they may have influenced tropical circulation (see section 2). On the western side of the Pacific, the northward movement of the Australian Plate and the associated development of the East Indies do not appear to have had a strong effect on the upstream Pacific equatorial circulation. However, the greater westward extent of the equatorial band of high productivity was not seen after the north coast of New Guinea reached latitudes less than about 10°S (cf. Figures 4–9). We did not use Indian Ocean sites in this study; however it would be interesting to pursue further studies that would reveal how the northward movement of the Australian and Indian Plates affected equatorial circulation in the trans Indian-Pacific Ocean region.

[40] The gradual closure of the Isthmus of Panama has frequently been cited as having a major impact on late Neogene circulation and climate in both the Atlantic and Pacific Oceans. Much less attention has been given this gateway in the Paleogene. Recently, *Huber and Sloan* [1999, 2000] conducted an ocean circulation model study that showed how flow through a relatively deep passage between the tropical Atlantic and Pacific Oceans might induce divergence of near surface waters and enhance productivity through the passage and perhaps downstream. This effect may account for the pattern of upwelling seen in the eastern equatorial Pacific of the Paleogene and fairly well predicted in *Huber*'s [2002] "Strawman" model. *Huber* [2002] acknowledges that the circulation model used does not deal particularly well with the ITCZ and that it tends to produce an overly strong southern ITCZ. The eastern boundary of the tropical Pacific is also more crudely represented in the model. Nevertheless, the patterns of upwelling produced by his model show some similarity to the patterns of equatorial sediment accumulation in the intervals older than 26 Ma.

[41] The plate reconstructions cited above (see section 2) for the Central American gateway indicate that its history is not a simple one with the Isthmus of Panama gradually swinging shut. Rather there was the potential for at least two and perhaps three separate gateways between the Caribbean and the Pacific. The Isthmus of Panama was the last of these to close (in the Pliocene). Prior to that, a passage between Nicaragua and Costa Rica closed sometime near 28 Ma according to the reconstruction used [*Hay et al.*, 1999] (Figures 6–8) and another narrow passage south of the Yucatan Peninsula (in the Guatemala-Honduras area) may have been open after ~32 Ma and before ~20 Ma [*Hay et al.*, 1999] (Figures 5–7). We do not know how deep these gateways may have been, but their existence does appear to have had an impact on equatorial circulation patterns. The well-developed northern equatorial tongue of high accumulation rates is only seen when one (or both) of these more northern gateways are open (Figures 6–11). In addition, the strength of the NEC/NECC zone seems best developed when the northern passages are wide.

[42] The early Eocene reconstruction (Figure 11) has ODP Leg 199 sites rotated into the extreme eastern tropical Pacific. These Leg 199 sites are all located on 56 Ma crust and lay above the very shallow CCD of that time. In the period of early Eocene peak warmth, sediment accumulation rates in the equatorial zone were 2 to 7 m/Myr (Sites 1219 and 1220). Accumulation rates in the northern

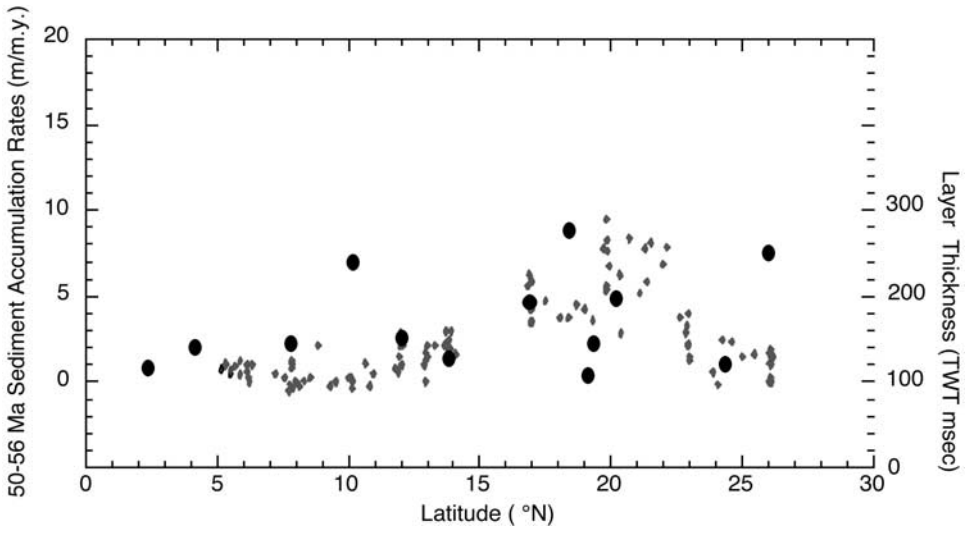

Figure 15. Sediment accumulation rates for the sites east of 160°W paleolongitude in the 50–56 Ma interval (filled dots; from Figure 12j) plotted versus modern latitude of the sites. Diamonds indicate discrete measurements of the thickness of the basal package of high-amplitude seismic reflections lying over 56 Ma oceanic crust [from *Moore et al.*, 2002b]. Thickness is measured in two-way travel time (TWT). See color version of this figure at back of this issue.

equatorial zone (Sites 1215 and 1216) are just as high over a broader area (Figures 11, 12j, and 13). This broad zone of higher accumulation rates distinctly north of the equator and the associated thicker early Eocene sediments of this region were first revealed by the analysis of seismic data taken along the 56 Ma crustal isochron [*Moore et al.*, 2002b]. Considering that the seismic estimates of thickness were made prior to any drilling in the area and that the sites are point measurements made not necessarily on the seismic transect, the comparison of the lower Eocene accumulation rates in ODP and DSDP sites (Figure 12j) with the independent seismic interpretation shows reasonably good agreement (Figure 15). As in our map of accumulation rates (Figure 11), the seismically estimated thickness of lower Eocene sediments show a broad area of higher accumulation rates (thicker sediments) in the northeastern tropical Pacific that drops off sharply north of about 27°N (modern latitude) [*Moore et al.*, 2002b].

[43] Combining the Leg 199 sites with other sites that sampled the early Eocene in the tropical Pacific seems to indicate that the northern sites of the Leg 199 transect lay where flow through the northern gateway and from the paleo-California Current would have had their strongest influence. Sediment accumulation there was, on average, greater than that found in the area of a much narrower and weaker equatorial divergence.

[44] Although the location of this tongue of higher accumulation rates north of the equator is consistent with the zone of divergence associated with the modern North Equatorial Current, such a clear impact on sediment accumulation is not seen in modern sediments. Nor is it seen in any of the reconstructions following the closure of the northern Pacific-Caribbean gateway(s). We suggest that the combination of the NEC/NECC divergence, divergent flow through the northern Caribbean-Pacific gateway(s), and possibly advective transport from the paleo-California Current, were sufficient to boost nutrient levels in the area of the North Equatorial Current to the point that it impacted the patterns of biogenic sedimentation. It is also possible that the source waters being upwelled in the northern divergence zone were richer in nutrients prior to 26 Ma than after that time. This impact is seen in the eastern tropical Pacific of early middle Eocene and early Eocene times even when average accumulation rates in the tropical Pacific were at their lowest (Figures 10, 11, and 13).

[45] The final major change in circulation patterns that may derive from changes in the boundaries of the Pacific basin lies in the South Pacific. In the younger reconstructions the only sites with accumulation rates above 10 m/Myr in the tropical and subtropical South Pacific are located on topographic highs. In the 26–30 Ma and older reconstructions, however, a broad area of relatively high accumulation rates is seen to extend from the southeastern South Pacific into latitudes of 10°–20°S. Although the patterns of sediment accumulation rates mapped in the South Pacific are based on only a few sites, the disappearance of this region of higher accumulation rates in the southeastern South Pacific seems to lie close in timing to the opening of the Drake Passage at about 31 Ma [*Lawver and Gahagan*, 2003]. We propose that this region of higher accumulation rates derives from circulation driven by relatively strong subpolar westerlies and Trade Winds of the southern subtropical region, deflected by the South America-Antarctic basin boundary, and advected northward from the (almost) Circumpolar Current. Once the Drake Passage did open and the Circumpolar Current became truly circumpolar, the flow from this source was diminished. The development of the Nasca Ridge and its subsequent subsidence may also have had a role in determining the exact pathway of flow northward into the South Pacific. Clearly such speculation

needs to be addressed by future scientific ocean drilling legs in the South Pacific.

5. Summary

[46] Averaging accumulation rates over 4 to 6 my has smoothed shorter term variability in these rates; however, the blurring of latitudinal zones of higher productivity likely amounts to about one degree of latitude (i.e., less than the width of the equatorial zone of high accumulation rates mapped in modern sediments). Variation through time in these average rates by a factor of 2 to 5 is seen in the equatorial band of high deposition rates. The highest equatorial rates are found in the Oligocene through Miocene times when the CCD was comparatively deep. However, a well-developed equatorial tongue of high rates is seen well into the Eocene. Although climate and the lithologic nature of the sediments change markedly across the Eocene-Oligocene boundary, the definition and extent of the equatorial zone of higher accumulation rates do not change. The two oldest intervals mapped span the time when Eocene climate was at its warmest, and it is during this time that the overall average accumulation rates were lowest and the equatorial divergence appeared to be less well developed.

[47] The most striking and surprising change in the patterns of sediment accumulation rates occurs in the Oligocene. Prior to this time there is a distinct zone of higher accumulation rates north of the reconstructed equator, which we associate with enhanced divergence at the NEC/NECC boundary (as suggested by *Huber* [2002]). The high accumulation rates in this zone may also be bolstered by divergence associated with flow through the northern gateways from the Caribbean. The average accumulation rates in this zone exceed those in the equatorial zone in the lower and lower middle Eocene; they are only slightly lower than average accumulation rates in equatorial zone for the rest of the Eocene. Even though the accumulation rates in the NEC/NECC zone drop at the Eocene-Oligocene boundary as rates in the equatorial zone continue to climb (Figures 12 and 13), the existence of this northern zone of higher accumulation rates persists into the Oligocene (Figures 5, 12e, 12f, and 13). In all younger reconstructions there is no evidence of higher accumulation rates associated with the divergence at the NEC/NECC boundary. In younger reconstructions the accumulation rate patterns are stable, showing a sharp drop off in accumulation rates to the north of the equatorial zone (Figures 12a–12d). The only variation found is the westward extent of the equatorial tongue and the magnitude of accumulation rates found within the equatorial zone (Figures 2–5 and 13).

[48] Surface circulation patterns as revealed by patterns of sediment accumulation suggest three major controls on the pattern of sediment accumulation in the tropical Pacific: 1) Variation in the strength of the trade wind system and/or near-surface density structure as evidenced by variation in average accumulation rates associated with zones of divergence; 2) Changes in the depth of the CCD, particularly the sharp drop in the CCD at the Eocene Oligocene boundary which increased average accumulation rates in the tropical Pacific; and 3) The opening and closing of oceanic gateways. The gradual closure of the Pacific-Indian Ocean tropical gateway may have affected the extent of the zone of equatorial divergence seen in the Pacific. The closing of one or more gateways between the Caribbean and Pacific during the Paleogene near 30 Ma appears to have been associated with the disappearance of the distinctive zone of higher accumulation rates north of the equator. This was also about the time that flow into the eastern South Pacific appears to have ceased to enhance accumulation rates in that region. This latter change in depositional patterns may have been associated with the opening of the Drake Passage.

[49] **Acknowledgments.** The authors thank the scientific party, technical staff, drillers, and ship's crew of the JOIDES Resolution for their hard work on ODP Leg 199. It was through their efforts that the critical data for this study were acquired. We also acknowledge support from the U.S. Science Support Program that funded the efforts of Moore, Nigrini, and Sanfilippo in this study. The senior author also acknowledges and thanks T. H. van Andel, who showed us the way 30 years ago.

References

Acton, G. D., and R. G. Gordon (1994), Paleomagnetic tests of Pacific plate reconstructions and implications for motions between hotspots, *Science*, *263*, 1246–1254.

Bohaty, S. M., and J. C. Zachos (2003), Significant Southern Ocean warming event in the late middle Eocene, *Geology*, *31*(11), 1017–1020.

Cande, S. C., and D. V. Kent (1995), Revised calibration of the geomagnetic polarity timescale for the Late Cretaceous and Cenozoic, *J. Geophys. Res.*, *100*, 6093–6095.

Christensen, U. (1998), Fixed hotspots gone with the wind, *Nature*, *391*, 739–740.

Duncan, R. A., and M. A. Richards (1991), Hotspots, mantle plumes, flood basalts, and true polar wander, *Rev. Geophys.*, *29*, 31–50.

Engebretson, D. C., A. Cox, and R. G. Gordon (1985), *Relative Motions Between Oceanic and Continental Plates in the Pacific Basin*, vol. 206, *Spec. Publ.*, Geol. Soc. of Am., Boulder, Colo.

Ewing, J. I., M. Ewing, T. Aitken, and W. J. Ludwig (1968), North Pacific sediment layers measured by seismic profiling, in *The Crust and Upper Mantle of the Pacific Area*, *Geophys. Monogr. Ser.*, vol. 12, edited by L. Knopoff, C. L. Drake, and P. J. Hart, pp. 147–173, AGU, Washington, D. C.

Fedorov, A. V., and S. G. Philander (2000), Is El Niño changing?, *Science*, *288*, 1997–2002.

Gordon, R. G. (1983), Late Cretaceous apparent polar wander of the Pacific plate: Evidence for a rapid shift of the Pacific hotspots with respect to the spin axis, *Geophys. Res. Lett.*, *10*, 709–712.

Gripp, A. E., and R. G. Gordon (1990), Current plate velocities relative to the hotspots incorporating the NUVEL-1 global plate motion model, *Geophys. Res. Lett.*, *17*, 1109–1112.

Hay, W. W., et al. (1999), Alternative global cretaceous paleogeography, in *The Evolution of Cretaceous Ocean/Climate Systems*, *Spec. Pap.*, vol. 332, edited by E. Barrera and C. Johnson, pp. 1–47, Geol. Soc. of Am., Boulder, Colo.

Heath, G. R., T. C. Moore Jr., and T. H. van Andel (1977), Carbonate accumulation and dissolution in the equatorial Pacific during the past 45 million years, in *The Fate of Fossil Fuel CO_2* in the Oceans, edited by N. R. Andersen and A. Malahoff, pp. 627–639, Plenum, New York.

Huber, M. (2002), Straw Man 1: A preliminary view of the tropical Pacific from a global coupled climate model simulation of the early Paleogene, *Proc. Ocean Drill. Program, Initial Rep.*, *199*, 1–30.

Huber, M., and R. Caballero (2003), Eocene El Niño: Evidence for robust tropical dynamics in the "hothouse," 299*, 877–881.*

Huber, M., and L. C. Sloan (1999), The challenges of modeling extreme warm climates:

Old problems, new models, *Eos Trans. AGU*, *80*(46), Fall Meet. Suppl., F488.
Huber, M., and L. C. Sloan (2000), Modeling the Paleogene; part II, Paleogene wind-driven ocean circulation changes predicted from climate modeling studies, *GFF*, *122*(1), 80–81.
Kono, M. (1980), Paleomagnetism of DSDP Leg 55 basalts and implications for the tectonics of the Pacific plate, *Initial Rep. Deep Sea Drill Project*, *55*, 732–752.
Lawver, L. A., and L. M. Gahagan (2003), Evolution of Cenozoic seaways in the Circum-Antarctic region, *Palaeogeogr. Palaeoclimatol. Palaeoecol.*, *198*(1–2), 11–37.
Liu, Z. Y., and B. Huang (1997), A coupled theory of tropical climatology: Warm pool, cold tongue, and Walker Circulation, *J. Clim.*, *10*, 1662–1679.
Lyle, M., et al. (2002), *Proceedings of the Ocean Drilling Program, Initial Reports* [CD-ROM], vol. 199, Ocean Drill. Program, College Station, Tex.
Mayer, L. A., et al. (1992), *Proceedings of the Ocean Drilling Program, Initial Reports*, vol. 138, Ocean Drill. Program, College Station, Tex.
Molnar, P., and J. Stock (1987), Relative motions of hotspots in the Pacific, Atlantic, and Indian Oceans since late Cretaceous time, *Nature*, *327*, 587–591.
Moore, T. C., Jr., A. Sanfilippo, and C. Nigrini, and the ODP Leg 199 Scientific Party (2002a), Early Cenozoic stratigraphy of the equatorial Pacific and the Eocene revealed, *Eos Trans. AGU*, *83*(47), Fall Meet. Suppl., F496.
Moore, T. C., Jr., D. K. Rea, M. Lyle, and L. M. Liberty (2002b), Equatorial Ocean circulation in an extremely warm climate, *Paleoceanography*, *17*(1), 1005, doi:10.1029/2000PA000566.
Petronotis, K. E., R. G. Gordon, and G. A. Acton (1994), A 57 Ma Pacific plate paleomagnetic pole determined from skewness analysis of crossings of marine magnetic anomaly 25r, *Geophys. J. Int.*, *118*, 529–554.
Pisias, N. G., L. A. Mayer, and A. C. Mix (1995), Paleoceanography of the eastern equatorial pacific during the Neogene: Synthesis of Leg 138 drilling results, *Proc. Ocean Drill. Program Sci. Results*, *138*, 5–22.
Sager, W., and U. Bleil (1987), Latitudinal shift of Pacific hotspots during the Late Cretaceous and early Tertiary, *Nature*, *326*, 488–490.
Sager, W., and M. S. Pringle (1988), Mid-Cretaceous to early Tertiary apparent polar wander path of the Pacific plate, *J. Geophys. Res.*, *93*, 1753–1771.
Shackleton, N. J., S. J. Crowhurst, G. P. Weedon, and J. Laskar (1999), Astronomical calibration of Oligocene-Miocene time, *Philos. Trans. R. Soc. London, Ser. A*, *357*, 1907–1929.
Steinberger, G. M. (1996), Motion of hotspots and changes of the Earth's rotation axis caused by a convecting mantle (Easter Island), Ph.D. dissertation, 203 pp., Harvard Univ., Cambridge, Mass.
Sun, D. Z. (2000), Global climate change and El Niño: A theoretical framework, in *El Niño and the Southern Oscillation*, edited by H. F. Diaz and V. Markgraf, pp. 443–463, Cambridge Univ. Press, New York.
Tarduno, J. A., and R. Cottrell (1997), Paleomagnetic evidence for motion of the Hawaiian hotspot during the formation of the Emperor seamounts, *Earth Planet. Lett.*, *153*, 171–180.
Tarduno, J. A., and J. Gee (1995), Large scale motion between Pacific and Atlantic hotspots, *Nature*, *378*, 477–480.
Tarduno, J. A., et al. (2002), *Proceedings of the Ocean Drilling Program, Initial Reports* [CD-ROM], vol. 197, Ocean Drill. Program, College Station, Tex.
Tarduno, J. A., et al. (2003), The Emporer Seamounts: Southward motion of the Hawaiian hotspot plume in the Earth's mantle, *Science*, *301*, 1064–1069.
van Andel, T. H., G. R. Heath, and T. C. Moore Jr. (1975), *Cenozoic History and Paleoceanography of the Central Equatorial Pacific Ocean*, *Geol. Soc. of Am. Mem.*, vol. 143, Geol. Soc. of Am., Boulder, Colo.
Zachos, J. C., L. D. Stott, and K. C. Lohmann (1994), Evolution of early Cenozoic marine temperatures, *Paleoceanography*, *9*, 353–387.
Zachos, J. C., M. Pagani, L. Sloan, E. Thomas, and K. Billups (2001), Trends, rhythms, and aberrations in global climate 65 Ma to present, *Science*, *292*, 686–693.

J. Backman, Department of Geology and Geochemistry, Stockholm University, Stockholm S-10691, Sweden.
M. Lyle, Center for Geophysical Investigation for the Shallow Subsurface, Boise State University, Boise, ID 83725, USA.
T. C. Moore Jr. and C. Nigrini, Department of Geological Sciences, University of Michigan, Ann Arbor, MI 48109-1063, USA. (tedmoore@umich.edu)
H. Pälike and I. Raffi, Dipartimento di Scienze della Terra, Universita G. D'Annuzio, Campus Univeritario, Chieti Scalo I-00040, Italy.
A. Sanfilippo, Scripps Institution of Oceanography, University of California, San Diego, La Jolla, CA 92093-0220, USA.

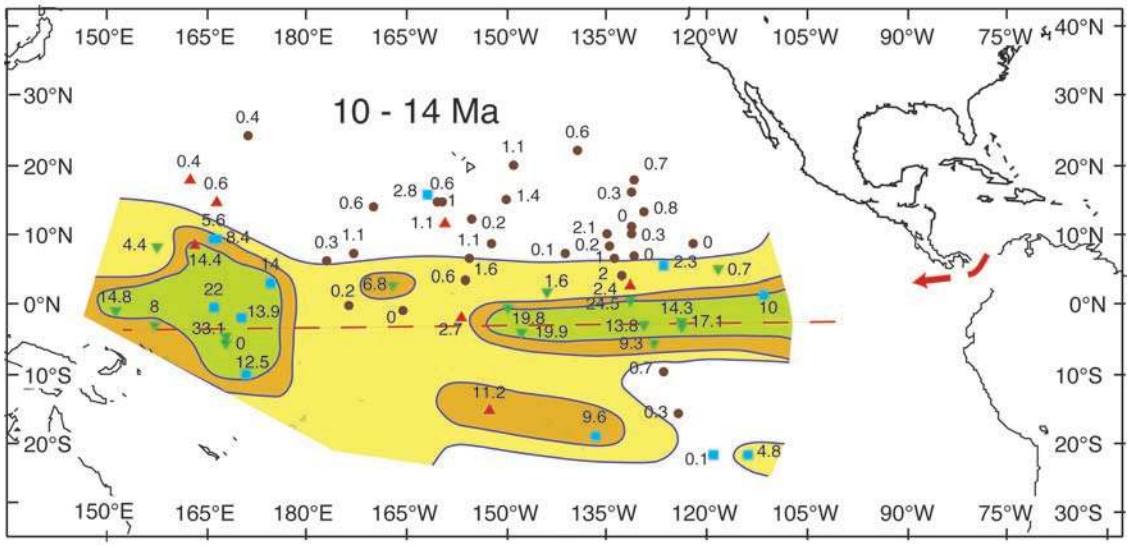

Figure 2. Average sediment accumulation rates for the interval 10–14 Ma given in units of meters per million years. Site positions are rotated to their estimated position at 12 Ma [*Engebretson et al.*, 1985; *Gripp and Gordon*, 1990]. Site location are marked and colored according to the microfossils used in the biostratigraphic reports for the time interval: filled squares (blue) show carbonate microfossils, inverted filled triangles (green) show siliceous and carbonate microfossils, filled triangles (red) show siliceous microfossils, and filled circles (brown) show clay or sparse siliceous microfossils. A red dashed line marks the approximate center of the equatorial divergence (geographic equator). Contours are at 1, 5, and 10 m/Myr.

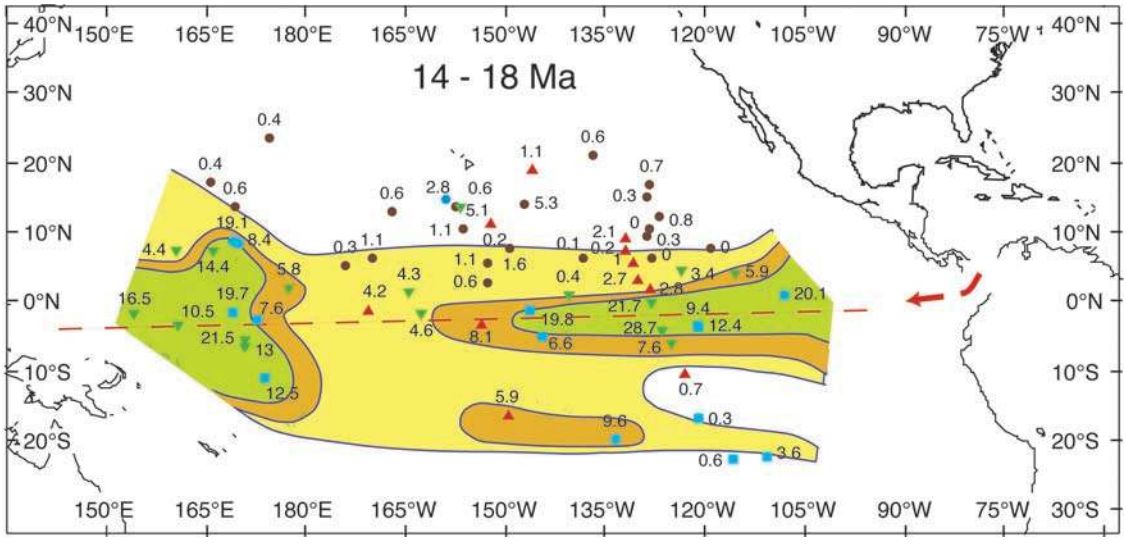

Figure 3. Average sediment accumulation rates for the interval 14–18 Ma given in m/Myr. Site positions are rotated to their estimated position at 16 Ma. Site location symbols and colors according to biostratigraphies used for the time interval. Symbols, colors, contours, and dashed line are as given in the caption to Figure 2.

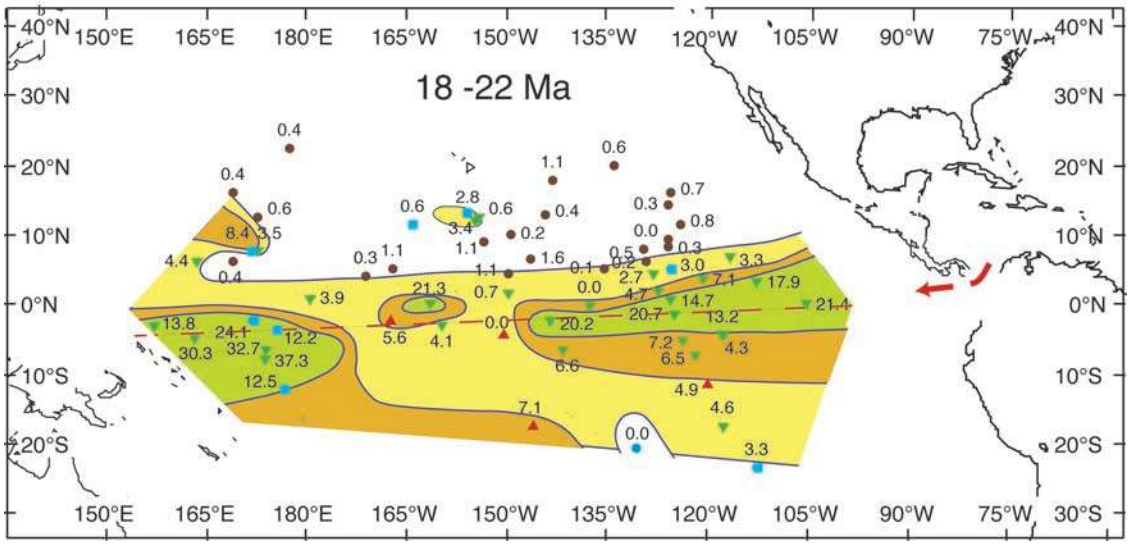

Figure 4. Average sediment accumulation rates for the interval 18–22 Ma given in m/Myr. Site positions are rotated to their estimated position at 20 Ma. Site location symbols and colors according to biostratigraphies used for the time interval. Symbols, colors, contours, and dashed line are as given in the caption to Figure 2.

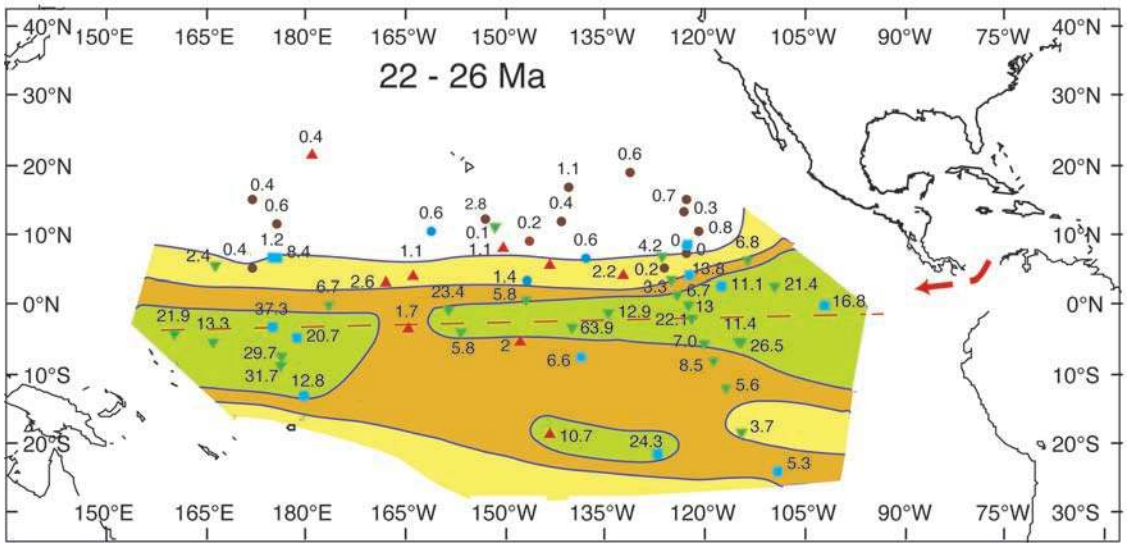

Figure 5. Average sediment accumulation rates for the interval 22–26 Ma given in m/Myr. Site positions are rotated to their estimated position at 24 Ma. Site location symbols and colors according to biostratigraphies used for the time interval. Symbols, colors, contours, and dashed line are as given in the caption to Figure 2.

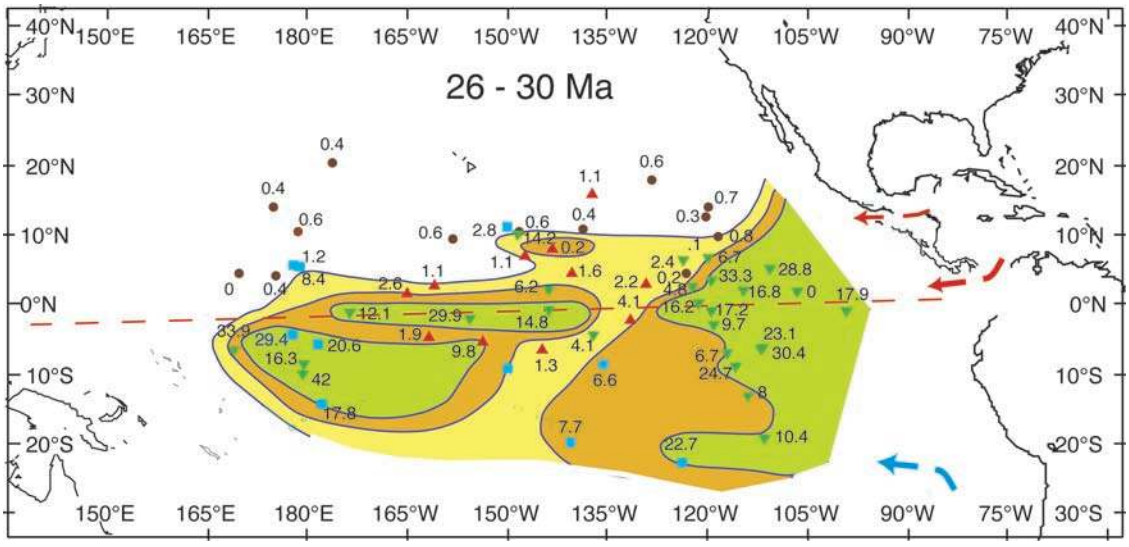

Figure 6. Average sediment accumulation rates for the interval 26–30 Ma given in m/Myr. Site positions are rotated to their estimated position at 28 Ma. Site location symbols and colors according to biostratigraphies used for the time interval. Symbols, colors, contours, and dashed line are as given in the caption to Figure 2.

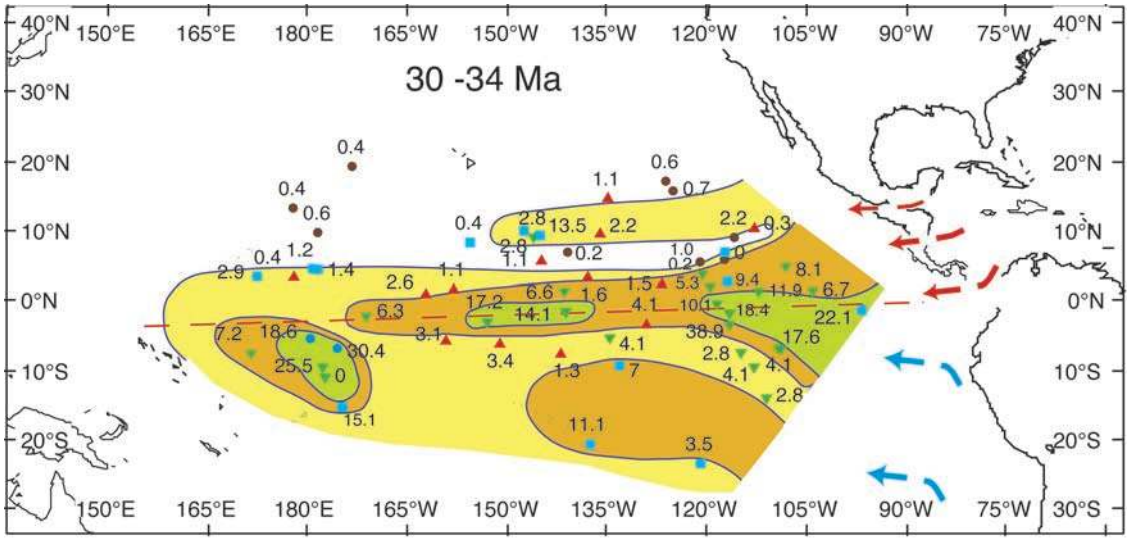

Figure 7. Average sediment accumulation rates for the interval 30–34 Ma given in m/Myr. Site positions are rotated to their estimated position at 32 Ma. Site location symbols and colors according to biostratigraphies used for the time interval. Symbols, colors, contours, and dashed line are as given in the caption to Figure 2.

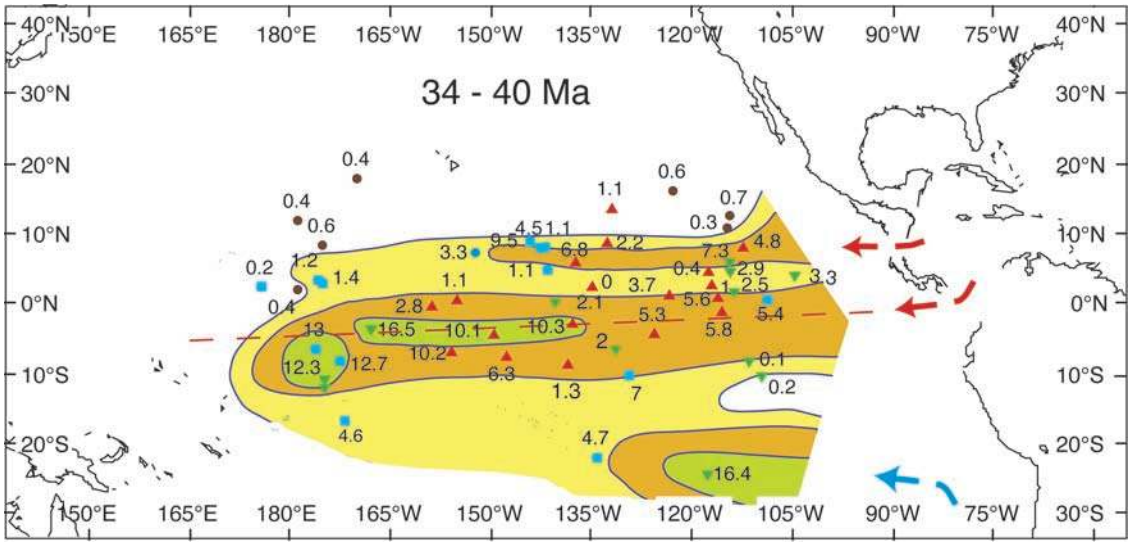

Figure 8. Average sediment accumulation rates for the interval 34–40 Ma given in m/Myr. Site positions are rotated to their estimated position at 37 Ma. Site location symbols and colors according to biostratigraphies used for the time interval. Symbols, colors, contours, and dashed line are as given in the caption to Figure 2.

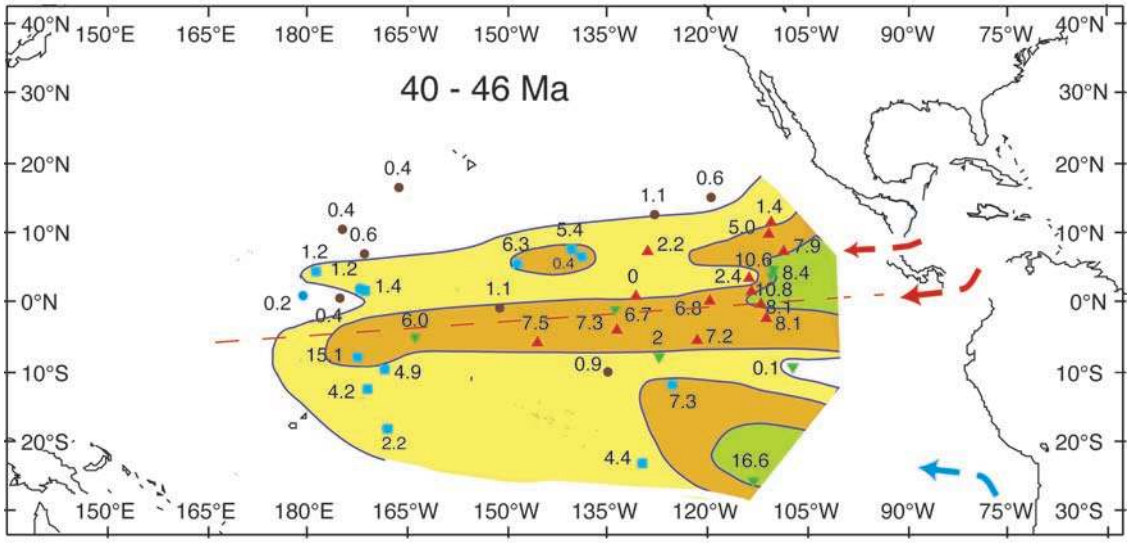

Figure 9. Average sediment accumulation rates for the interval 40–46 Ma given in m/Myr. Site positions are rotated to their estimated position at 43 Ma. Site location symbols and colors according to biostratigraphies used for the time interval. Symbols, colors, contours, and dashed line are as given in the caption to Figure 2.

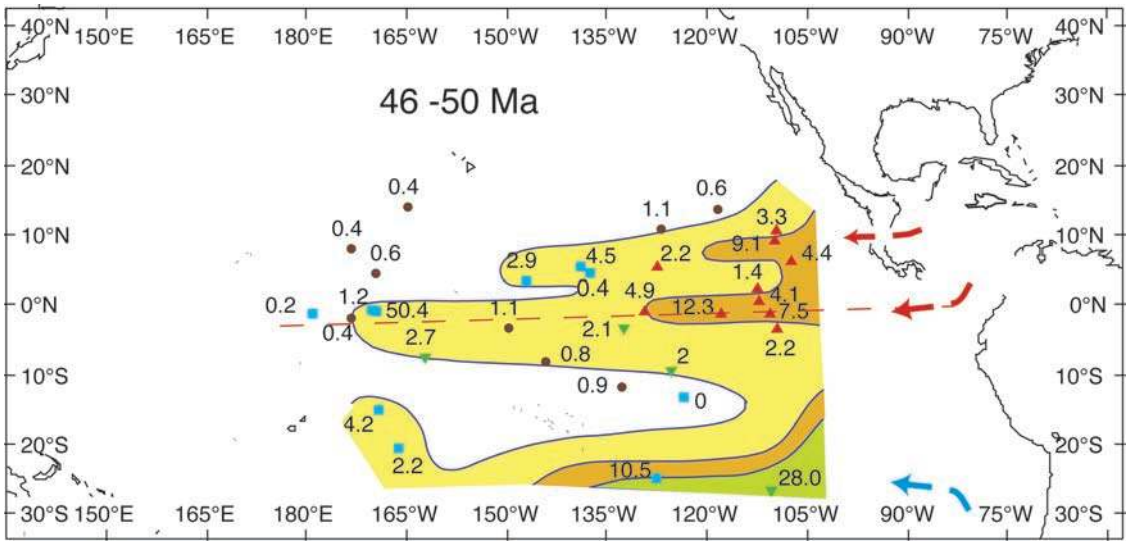

Figure 10. Average sediment accumulation rates for the interval 46–50 Ma given in m/Myr. Site positions are rotated to their estimated position at 48 Ma. Site location symbols and colors according to biostratigraphies used for the time interval. Symbols, colors, contours, and dashed line are as given in the caption to Figure 2.

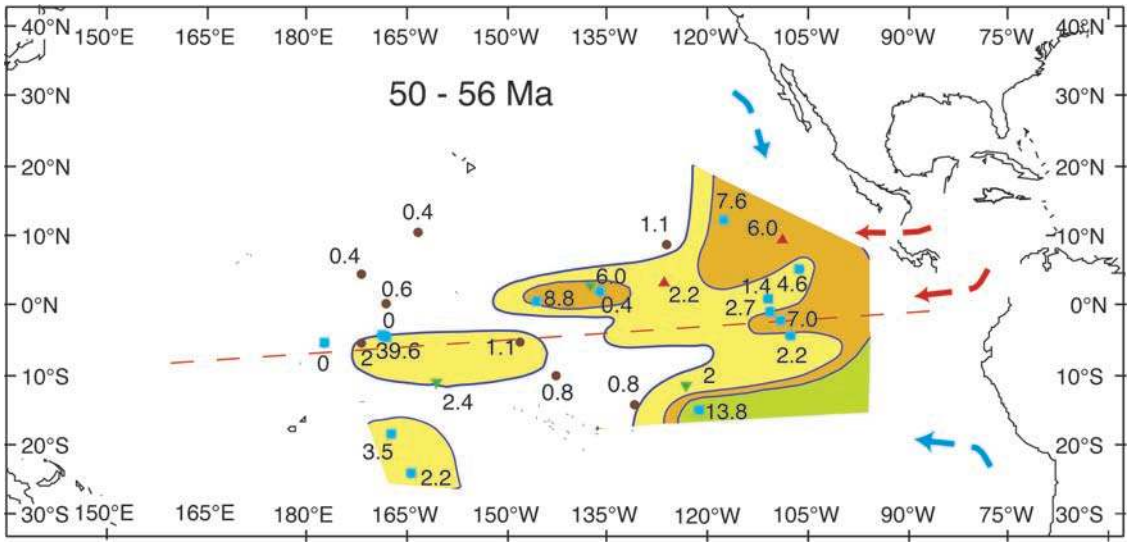

Figure 11. Average sediment accumulation rates for the interval 50–56 Ma given in m/Myr. Site positions are rotated to their estimated position at 53 Ma. Site location symbols and colors according to biostratigraphies used for the time interval. Symbols, colors, contours, and dashed line are as given in the caption to Figure 2.

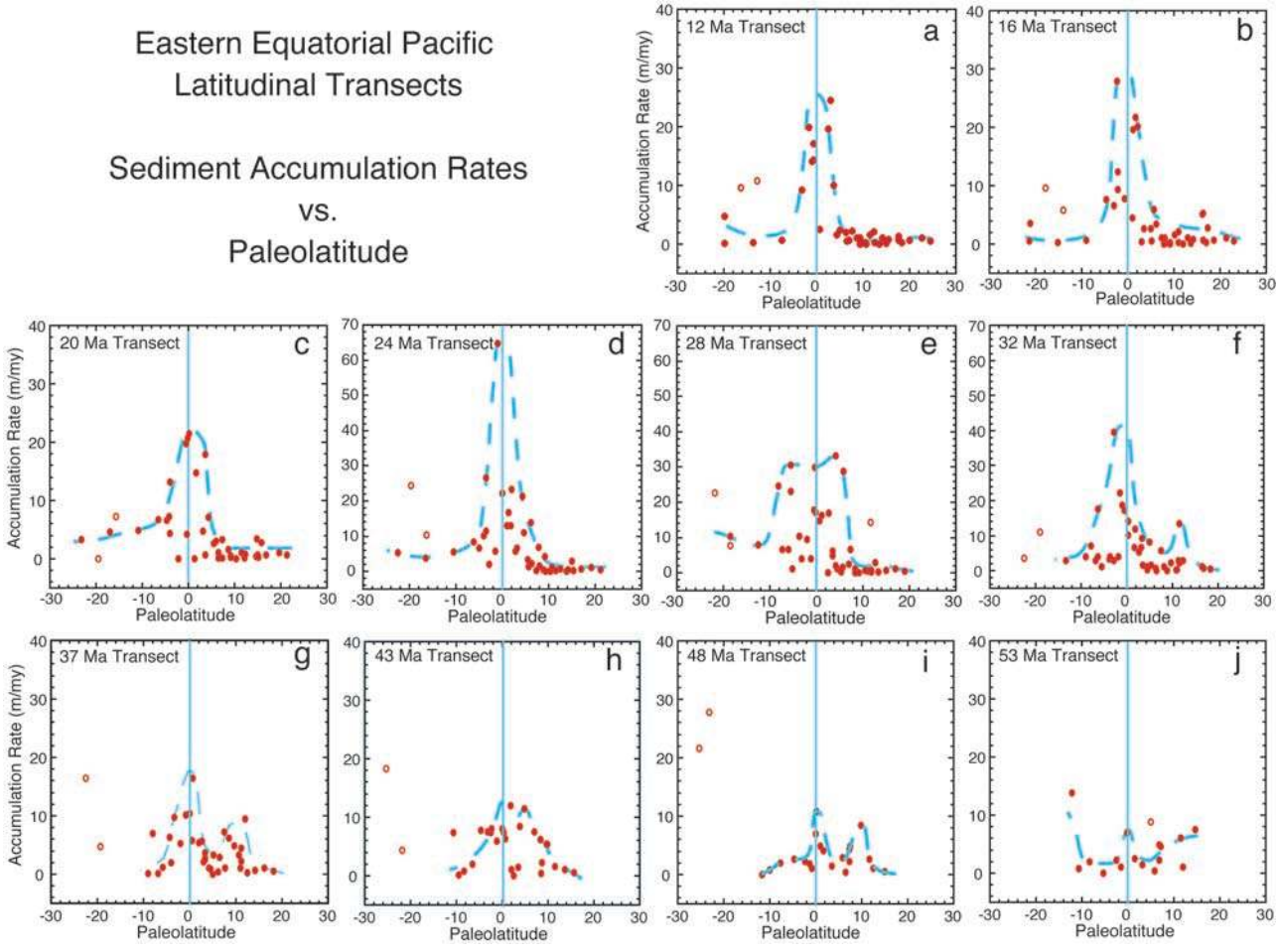

Figure 12. Sediment accumulation rates for sites east of 160°W paleolongitude plotted versus the site paleolatitude for each reconstructed time interval. Open circles indicate sites drilled at <3000 m water depths. Paleolatitudes are measured relative to the paleoequator as defined by the dashed line through the center of the equatorial zone of higher accumulation rates in Figures 2–11.The vertical line marks the estimated position of the maximum equatorial divergence (i.e., the "geographic equator"). The dashed line outlines the higher accumulation rates seen in each transect. On the basis of the paleolatitude of the sites in each reconstruction and on the averaging effect of accumulation rate estimations, the estimated position of the geographical equator could have an error of about ±1° of latitude.

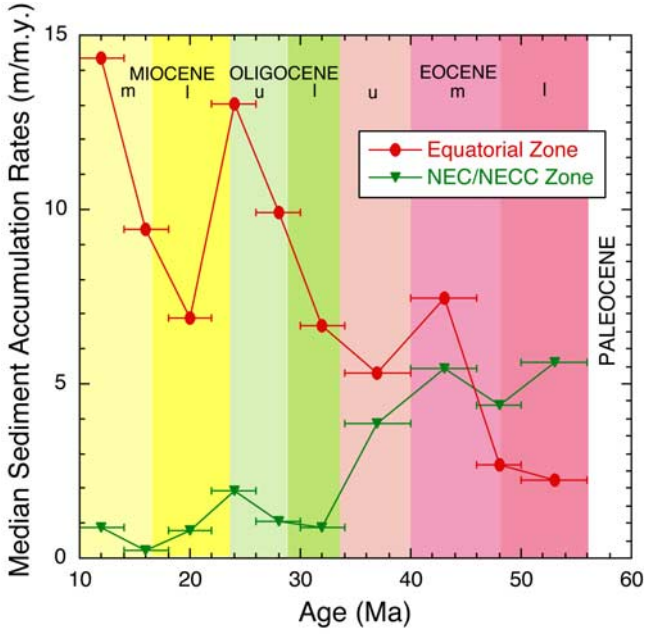

Figure 13. Median sediment accumulation rates for sites east of 160°W paleolongitude in the equatorial zone of high accumulation rates (~4°N–4°S; filled circles) and in the northern (NEC/NECC) zone (~6°–10°N; filled inverted triangles) for each of the ten reconstructed time intervals. Horizontal bars indicate length of each time interval over which accumulation rates are averaged.

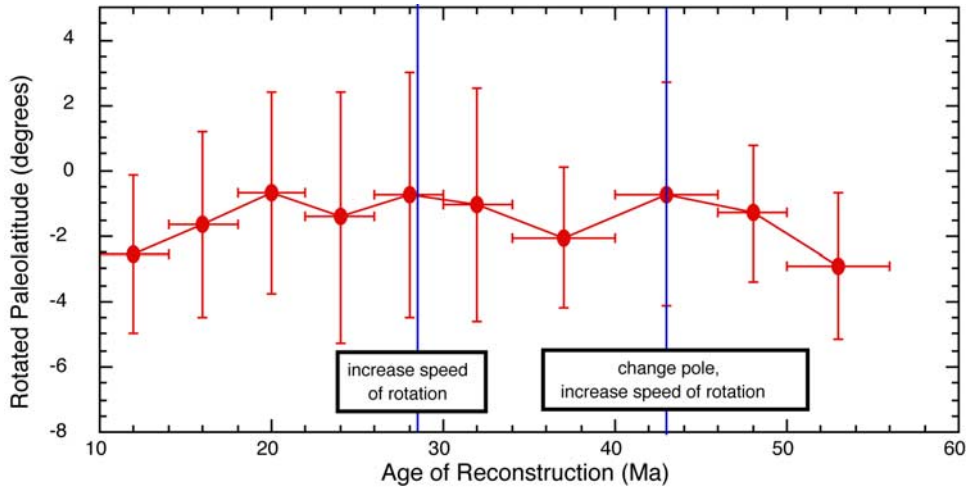

Figure 14. Rotated latitudinal position of geographic equator at 120°W paleolongitude. Geographic equator defined by equatorial zone of high accumulation rates and marked by dashed lines in Figures 2–11. Horizontal bars indicate length of each time interval over which accumulation rates are averaged. Vertical bar indicates width of equatorial zone of high accumulation rates. Vertical lines indicate times at which either the pole of rotation or angular speed of rotation changed in the rotation model [*Engebretson et al.*, 1985].

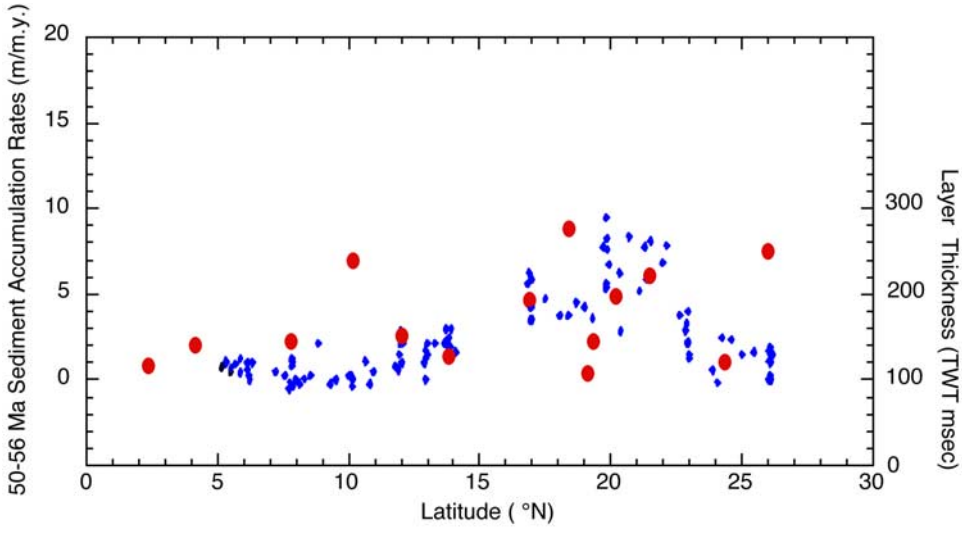

Figure 15. Sediment accumulation rates for the sites east of 160°W paleolongitude in the 50–56 Ma interval (filled dots; from Figure 12j) plotted versus modern latitude of the sites. Diamonds indicate discrete measurements of the thickness of the basal package of high-amplitude seismic reflections lying over 56 Ma oceanic crust [from *Moore et al.*, 2002b]. Thickness is measured in two-way travel time (TWT).